2017-01-01

Characterization Of Electrically Conductive Inks In Simulated Space Environment

Kazi Md Masum Billah
University of Texas at El Paso, masum.me106@gmail.com

CHARACTERIZATION OF ELECTRICALLY CONDUCTIVE INKS IN SIMULATED SPACE ENVIRONMENT

KAZI MD MASUM BILLAH

Master's Program in Mechanical Engineering

APPROVED:

Ryan Wicker, Ph.D., Chair

Arifur R. Khan, Ph.D.

David Roberson, Ph.D.

Jack Chessa, Ph.D.

Charles Ambler, Ph.D.
Dean of the Graduate School

Dedication

I would like to dedicate this thesis to my father Kazi Md Mofazzal Hossain, mother Mosa Nurun Nahar and my wife Tamanna Ferdous.

CHARACTERIZATION OF ELECTRICALLY CONDUCTIVE INKS IN SIMULATED SPACE ENVIRONMENT

by

KAZI MD MASUM BILLAH, BSc. in Mechanical Engineering

THESIS

Presented to the Faculty of the Graduate School of

The University of Texas at El Paso

in Partial Fulfillment

of the Requirements

for the Degree of

MASTER OF SCIENCE

Department of Mechanical Engineering

THE UNIVERSITY OF TEXAS AT EL PASO

August 2017

Acknowledgements

I want to express my gratitude to my supervisor and mentor Dr. Ryan Wicker, director of the W.M. Keck Center for 3D Innovation (Keck Center), for his continuous support, encouragement, guidance and constructive comments throughout my research as a graduate student. I would like to thank Dr. Arifur Khan research assistant professor at cSETR and Mr. David Espalin, manager of the Keck Center, for their continuous support in the research, his contribution of many ideas and encouraging me in different aspects. I would like to thank Dr. Ahsan Choudhuri, chair of the Mechanical Engineering Department for the continuous financial support. Also, I like to express my gratitude to him to give me the permission for using thermal vacuum chamber in cSETR. This research would not have been possible without the enormous research facility in Keck Center, expanded recently to over 13,000 sq. ft. and which provided access to state-of-the-art facilities and equipment as a result of funding from the State of Texas Emerging Technology Fund. I would like to thank my committee members, Dr. Jack Chessa and Dr. David Roberson. I would like to thank the former students, present students, and staff in the Keck Center and cSETR. My special thanks goes to Mr. Mohammed Shojib Hossain, Mr. Syed Zia Uddin, Mr. Naim Zahangir, Mr. Alfonso Fernandez, Ms. Mireya Perez, Mr. Mahesh Tonde, Gerrardo Olvera and Mr. Luis A. Ochoa for their help in various aspects.

Finally, I would like to thank my parents and my wife for their continuous support and encouragement.

Abstract

Increasing numbers of satellite missions necessitate a standalone power supply with self-recovery capabilities in case of failure in the space environment. A self-repairing kit was developed with the capabilities to repair the damaged solar array by dispensing conductive inks. Dispensing of conductive materials using direct writing technology to the space environment not only repairs damaged electronic components but also demonstrates the possibilities of manufacturing in outer space. For earth application, properties of direct writing inks have been evolved. In space application, direct writing inks or conductive inks have some issues such as outgassing, vapor pressure, curing etc.Therefore, having the properties known of electrically conductive ink can be used for dispensing materials in future space application. This research deals with the curing behavior of electrically conductive inks in simulated space environment.

For the experimental investigation, two types of electrically conductive ink E1660 (Ercon) and CB102 (DuPont) have been chosen which passed the requirements of NASA low outgassing (according to ASTM E595 test, condensed volatile collected mass is less than 0.1%). Also, both of the inks were studied previously as direct writing inks on a 3D printed substrate. E1660 and CB102 consist of flake based silver particles and nano silver particles respectively. A microdispenser was developed to demonstrate the ink injection on a customized printed circuit board. A simple and low-cost continuity test method was used to demonstrate the conductive behavior of inks at different temperatures and pressures at the representative of simulated space environment.

A thermal environment test that had the ability to create the temperature range from -150°C to 350°C was chosen to verify the experimental methods and procedure. Continuity test and voltage divider rule were employed together to determine the time required to develop a conductive path

on the surface and subsurface of the ink trace after being dispensed on the substrate. Time was measured until the maximum conductivity obtained for each test. Subsequently, to simulate the space environment, a thermal vacuum chamber was chosen that had the capability to create low vacuum pressure (10^{-2} Torr) and thermal cycle (-80℃ to 100℃). Thermal vacuum testing was used to examine the curing properties of conductive inks in a vacuum environment. For each thermal vacuum test, there was some bubble formation on the ink surface. Therefore, it was essential to study the microstructure of the cured ink after vacuum testing. SEM micrograph and LabVIEW machine vision tool were used to determine the void space that was created due to the evaporation of polymer binder or solution form the ink bulk. Though 10^{-2}Torr vacuum level is not exactly representing the deep space environment, this thesis provides the necessary information to develop a direct writing repair kit and characterization techniques of commercially available and previously studied inks.

Table of Contents

List of Tables

List of Figures

Chapter 1: Introduction

1.1 Introduction

Number of spacecraft is increasing day-by-day and it is adding more and more space debris. According to national aeronautics and space administration (NASA) data as of July 2016 [1], more than 500,000 pieces of trackable space debris are orbiting the earth. Space debris consists of both natural (meteoroid) and man-made particles. Only the man-made space debris is trackable in space whereas natural micrometeoroid is not. As a space shuttle leaves the earth, it enters the low earth orbit (LEO) first. *Figure 1* is representing the geocentric orbit locations depending on the distance from earth's surface (sea level). Medium earth orbit (MEO) spans from the end of LEO (2000km) to starting of geostationary earth orbit (GTO at 35786km) [2]. With the entry of a space shuttle to each geocentric orbit, the collision takes place with high velocity (7223m/s) debris [1]. Thus, it is not always possible to return back to earth with the same parts. It refers that some parts and materials are lost in space because of collision with space debris. This collision phenomena behaves as a chain as one broken part collides with other and leads to damage of other parts of

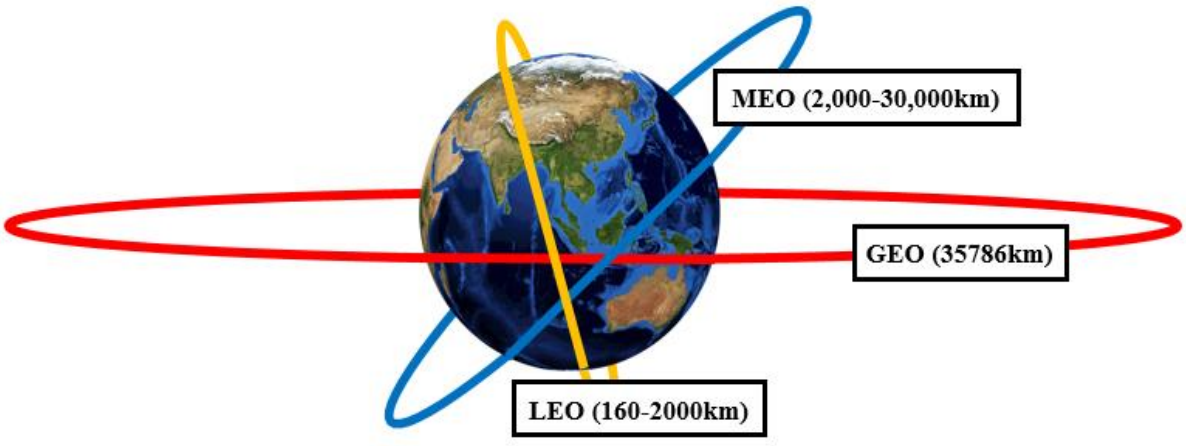

Figure 1: Classification and location of geocentric orbits based on the distance from the earth's surface (sea level) [2].

Table 1: Space environment characteristics

Space Environment	Sea Level	Low Earth Orbit	Medium Earth Orbit	Geostationary Earth Orbit
Temperature (˚C)	-40 to 40	-10 to 60	-20 to 75	-150 to 150
Pressure (Torr)	760	10^{-2} to 10^{-6}	10^{-5} to 10^{-8}	10^{-6} to 10^{-11}

space vehicle or space station. Space environment hazards such as electrostatic forces, ultraviolet irradiation etc. are responsible for damaging and malfunctioning of electronic components (e.g. antenna, solar array). Damage of a solar panel is a major concern for a space vehicle. In space, solar energy is the only power source and solar panels provide the means to collect solar energy and convert it into electrical energy.

Since solar panels are the key to derive electricity from sunlight to power a space system, damage to solar panels may lead to failures of the mission of space systems such as satellite, cube satellite, or space station. The damage to solar panels can be caused by space debris or the long-term exposure to the harsh space environment. *Table 1* represents the temperature and pressure ranges in the space environment. Primarily the space environment consists of the UV radiation, high vacuum, charged particles or plasma, and a wide range of temperature. Earth's atmosphere filters out the UV ray of solar radiation and the plasma environment is located above the earth atmosphere. Plasma environment consists of equal positively and negatively charged particles.

Continuous deposition of charged particles on the surface of materials in space environment can generate high potential voltage and heat flux. The potential voltage difference between materials surface and subsurface degrades the materials property and ultimately leads to failure in space. Radiation environment in space leads the UV irradiation of electron and trapped particles on the surface and subsurface of a material to degrade the material properties. Therefore,

the materials in space environment degrade with elapsed time. Solar panel of a satellite is always exposed to space environment. The space environment degrades the materials of the solar panel. According to the experimental investigation [3] and mission in space, the junction points between the arrays of the solar panel were mostly vulnerable and destroyed due to the exposure in space environment. Figure 2 represents a typical damaged solar panel junction of STS120 mission [2]. Also, the long-term exposure to the different orbit of the space environment such as Low Earth Orbit (LEO), Medium Earth Orbit (MEO), and Geostationary Transfer Orbit (GTO) has a detrimental effect on the solar panel [4, 5, 6].

According to the authors in [7], charging and discharging are also often factors to initiate the damage in microelectronics and solar panel of a satellite. Space grade shielding materials that

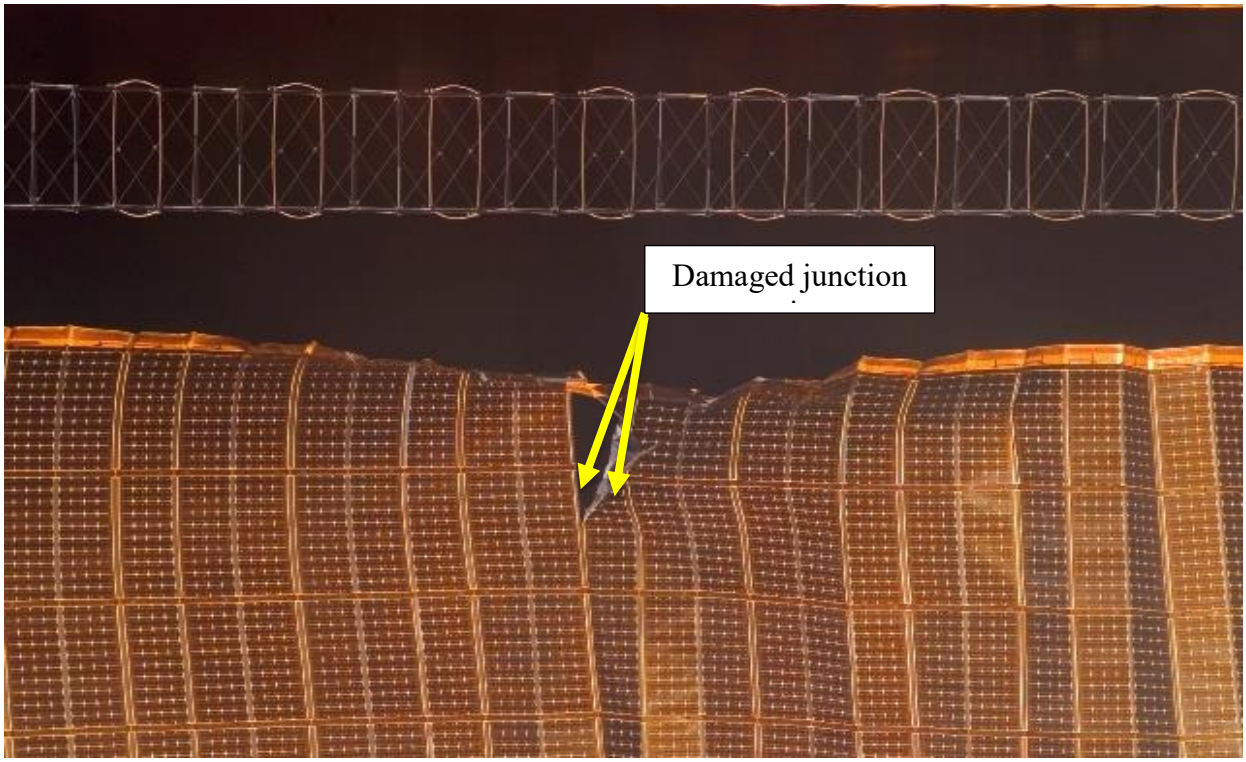

Figure 2: Photo of a damaged junction point P6 solar array on 4B wing of STS120 mission. The damage was found after the redeployment from original position of the vehicle [3].

have the ability to prevent UV irradiation, and electron emission, can be used to mitigate the damage and failure of microelectronics in space. But the solar panel damage cannot be mitigated as the shielding materials on panel surface reduce the efficiency of solar cell.

The authors in [8], presented the cost associated with the insurance of various parts of a satellite. A highest 33% of insurance claimed by only the malfunctioning of solar panel. In each satellite, solar panel takes about 30% of the total cost. If there is no malfunctioning or damage on the solar panel, then a major part of entire mission cost will be greatly reduced. Therefore, having the unavoidable factors of space hazards, there is a necessity to develop a solar panel or any electronics component repair kit. Direct writing is an unique idea to repair the damage by joining the terminal of solar cell with electrically conductive materials. Deposition of conductive materials

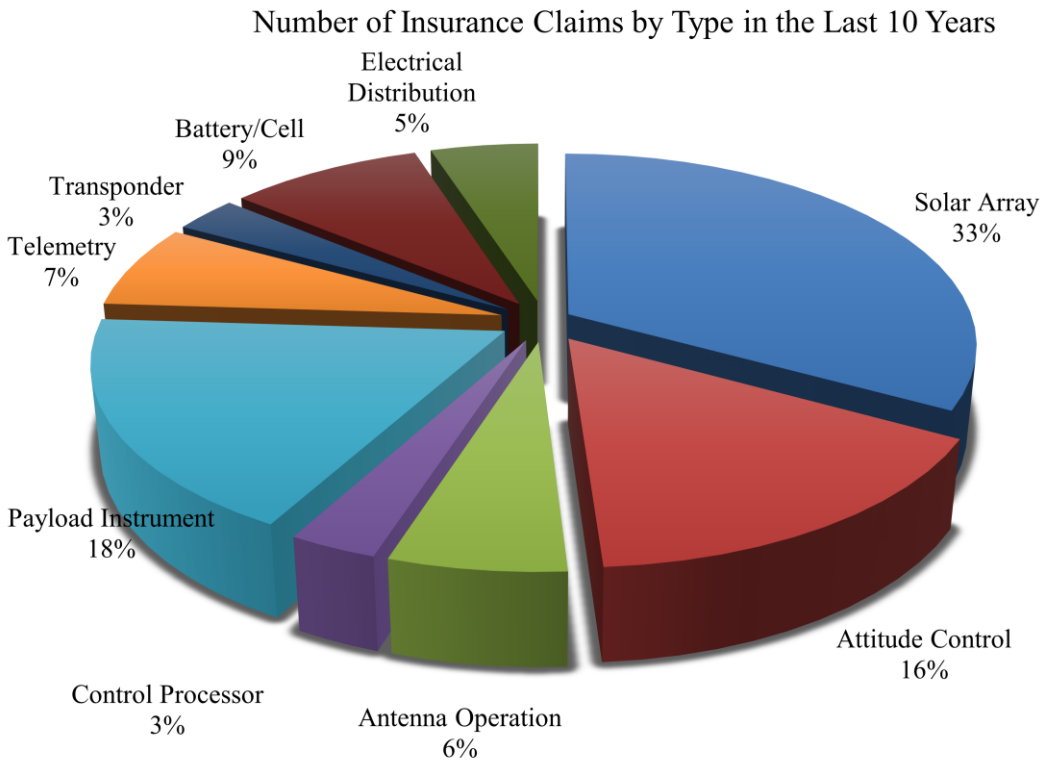

Figure 3: The pie chart shows a break-down of insurance claim for different malfunctioning in satellite operations. A highest 33% claim against solar array damage represents the high stakes involved with the loss of power supply which could be repaired with conductive inks

layer-by-layer or direct writing can fix the problem of loss of conductivity and make the damaged part fully functional. Therefore, there is a need for a system that dispenses conductive materials. Future additive manufacturing with the combination of direct writing of conductive materials in space, as well as the characterization of printable materials in a low vacuum environment, is an emerging research field.

Electrically Conductive Ink (ECI) characterization, has evolved greatly since its first use in the printing of electronic technology. Results of the applied curing method and limitations imposed by the curing environmental conditions indicated the final application. Printed electronics that consist of ECI, are made by either conventional printing technology (2D printing e.g. inject printing on paper) or direct write (DW), which this manuscript focuses on. However, the versatility of ECI in terms of the deposition parameters as well as, electrical, mechanical and morphological properties are the driving force for the use of DW technology to fabricate electrical and electronic prototypes. Though, ECI is highly used in the field of printed electronics [9], printed optics [10] and medical applications [11], until now no evidence was found to study the conductive ink characterization in low vacuum or space environment. Therefore, there is a need to further study on the conductive path development methods in space environments.

Space environment refers to temperatures ranging between -150˚C and 150˚C, pressure ranges of 10^{-2} Torr to 10^{-10} Torr, Coronal Mass Ejection (CME) from the sun, magnetic field fluctuation, high energy particles (charged or neutral) [12]. Electronic components that are made for space environments are usually manufactured in atmospheric conditions and followed by post manufacturing operations such as heat treatment, polishing, lapping to produce space-grade components. These techniques are used to prolong the durability of the components and allow the material to withstand the harsh environment. However, there is very limited research on the

manufacturing or repairing of electronic parts that are durable in harsh environments. Due to the different properties of each material, there are some challenges on the durability and qualifications of materials applicable for such space environment conditions. Outgassing from electronic chips or surrounding materials in space is one of the most common phenomena of physical deterioration because it causes electrostatic discharge during operation or thermal cycling. For the past four decades, there have been many research and industrial efforts to try to prevent outgassing after the complete solidification of the liquid materials. There are some commercially produced ECIs (silver ink from DuPont, silver contained adhesive from Thorlab Inc., and epoxy based silicon-silver conductive paste from Master Bond) available which can be applied to extreme environments only after complete solidification. Currently, manufacturing processes of space-grade parts are done at earth-based in-house facilities of industry or research laboratory. However, no electronic parts are currently being fabricated in space conditions, due to inability or lacking facilities specializing in the characterization of commercial inks while under thermal vacuum conditions. Data and observations of conductive trace in a thermal vacuum system can lead to new innovative electronic fabrication processes and repair of the damaged component that can be executed in space environments.

Space environment can be simulated in a vacuum system to create a low vacuum, thermal cycling, UV irradiation (high or low energy electron irradiation), and other relevant conditions [13]. Under these conditions, the durability of ECIs can be tested and recommendations can be made for space applicability, especially to repair the damaged electronic components of a satellite.

1.2 Motivation

ECI can be used as a material for direct writing to repair conductive trace between two junction point of electronic components in space. The variation in mechanical, electrical, and

thermal properties of ECIs are demonstrated adequately by testing in atmospheric condition. According to the specific requirements, ECIs can be selected and manufactured the desired parts. Continuous effort on the characterization of ECI research work has been carried out to obtain the desired properties within fabricated parts or electronics [14, 15]. Improved properties have been achieved after manufacturing of electronics and electrical parts only because of the evolved curing characterization and post curing operations. A better understanding of material properties during curing and post curing (in operation) is helpful when selecting the appropriate materials for manufacturing. This is because different metallic ink or materials have different curing time and mechanical properties. These parameters can affect the performance and quality as well. Since there is no research work on curing characterizations of ECI in a vacuum condition, there is an immense scope to investigate the curing phenomena in a thermal vacuum environment. Investigation of ECI curing phenomena in thermal vacuum condition will explore the possible opportunity of future manufacturing and repair in outer space. Curing of ECI in the space environment depends on several parameters such as the temperature, pressure, radiation environment, and so on. Therefore, this research will provide a better understanding of the conductive path development in the ink trace after being dispensed on a substrate., post curing properties and the potential application of ECI in the space environment. There are three main phases of this research work. First, the experimental study demonstrated the conductive behavior of selected ECIs in atmospheric condition. Second, the similar experimental procedure was employed in simulated space environment. Simulated space environment was made in a thermal vacuum chamber. The thermal vacuum system consists of the elevated temperature and low temperature testing facilities. To demonstrate ECI dispensing parameters such as trace thickness, width, and length, a micro dispensing system is needed, which dispenses the ECI on customized

PCB substrate. This micro dispenser works similar to an extruder of the three-dimensional printer because the printed trace is the addition of the materials layer by layer on PCB which defines the additive manufacturing as well as the three-dimensional direct writing. Thirdly, the post curing characterization such as continuity data analysis, SEM image analysis demonstrated the microstructural changes and conductivity mechanism through the flakes and Nano particles of the ink trace.

1.3 Thesis objectives

Space applicable printed electronics, shielding parts of satellite electronics and space shuttle repair kit as a conductive materials filler in space are the next generation technology, which is depending on the ECIs to obtain the sustainable as well as the reliable solution in space. The primary goal of this research was to develop a method of testing the conductivity properties of liquid inks after being dispensed on a substrate such as the time required to develop a conductive path, pressure, temperature etc. in a simulated space environment. Also, the ability to print the ECI or conductive paste using a micro dispenser demonstrated in the thermal environment but further investigation is needed in actual space environment in future. Meanwhile, this research work demonstrated the technique of dispensing the ink in a thermal environment which could be useful in further ground testing and simulated space environment testing of the space applicable materials. The overall research objectives of this thesis are following:

1. Development of spring loaded micro dispensing system to inject the ECI in simulated space environment.
2. Characterize the behavior of conductive ink and paste in thermal environment (at atmospheric pressure 760 Torr) and thermal vacuum environment (at vacuum pressure 10^{-2} Torr).

3. Investigate the possibility of ECI as the future direct writing of conductive material for space application.
4. Demonstrate the potential application of ECI as conductive materials with injector as payload of a 1U CubeSat.

The first objective serves the dual purpose in such a way that it can be used to dispense the liquid ink or paste in thermal vacuum system and similar mechanism can be used in space to demonstrate the direct writing technology and future AM. Rest of the objectives are the complementary for 3D printable electronics either in regular use in earth environment or the space environment.

1.4 Thesis outline

Overall structure and contents of the thesis are described as follows. Literature review at chapter 2 presents the past researches which have studied the curing characterization of ECI in atmosphere (sea level). Also, the space environment and thermal vacuum system have been described in this chapter to discuss the possible opportunity of direct writing of electrically conductive ink and future AM in simulated space environment. Chapter 3 represents the methods and experimental procedures. The method of the conductive path development discusses the various techniques and mechanisms to accomplish the thesis objectives. The experimental procedure and test setup provide a model for the overall test procedure and facility for simulated space environment and atmospheric testing. Additionally, the material selection, thermal testing, electrical instrumentation and data acquisition procedures are discussed. Results and discussion in chapter 4 present the findings of curing parameter in a thermal environment chamber (at 760 Torr), thermal vacuum chamber (at 10^{-2} Torr). Additionally, the surface structure or morphology and

limitations associated with the existing experimental setup was also discussed. Finally, in chapter 5 the conclusions and recommendations to implement in future work are provided.

Chapter 2: Literature Review

2.1 Introduction

According to ASTM F2792-12a standard terminology, additive manufacturing (AM) is a process of joining materials to make objects from 3D model data, usually layer upon layer as opposed to subtractive manufacturing methodologies [16]. Comparing to the traditional manufacturing techniques that can create a prototype using significant number of process and methods, rapidly grown AM technology takes the prototype fabrication to the next level by accomplishing followings: (a) complexity is free, (b) no assembly, (c) variation in design, (d) infinite shades of materials, (e) integration of multiple operations, and (f) less constraints. Initially, AM were limited to prototyping, but improvements of design parameters, mechanical properties, post processing have allowed the wide range of customization in structural parts and components fabrication [17]. AM technology comprises of seven different categories. A brief description of all seven categories offered in next sentences [16]. (i) Binder jetting, an AM process in which a liquid bonding agent is selectively deposited to join powder materials. (ii) Material jetting, an additive manufacturing process in which droplets of build material are selectively deposited. (iii) Directed energy deposition, an AM process in which focused thermal energy is used to fuse materials by melting as they are being deposited. (iv) Material extrusion, an AM in which material is selectively dispensed through a nozzle or orifice. (v) Sheet lamination, an AM process in which sheets of material are bonded to form an object. (vi) Vat photopolymerization, an AM process in which liquid photopolymer in a vat is selectively cured by light-activated polymerization. And (vii) Powder bed fusion, an AM process in which thermal energy selectively fuses regions of a powder bed. To obtain 3D objects using AM technology following common steps need to be done. The first step is to make a CAD file of the desired object and convert it to a STL file. The second step

is to send the tooling command from STL file to the AM machine. AM machine builds the 3D part layer by layer. The final step is to remove the part from AM machine and post processing if required. Though there are various types of AM technology available for parts fabrication, author of this thesis uses only a part of material extrusion technology to fabricate and repair electronics components.

Electrical parts such as Printed Circuit Board (PCB) can be manufactured using the combination of 3D printing technology and direct writing technology. For example, a 3D printed substrate that has predesigned trenches on the body can be used to fabricate functional and structural electronics. The pre-designed trenches on the substrate are filled out with the deposited ECI using an extruder head that can dispense conductive ink. Deposition of ECI on trenches or pre-specified paths need two major components. Firstly, a computer controlled translation stage helps to generate a pattern of conductive ink on a substrate. Secondly, an ink deposition nozzle

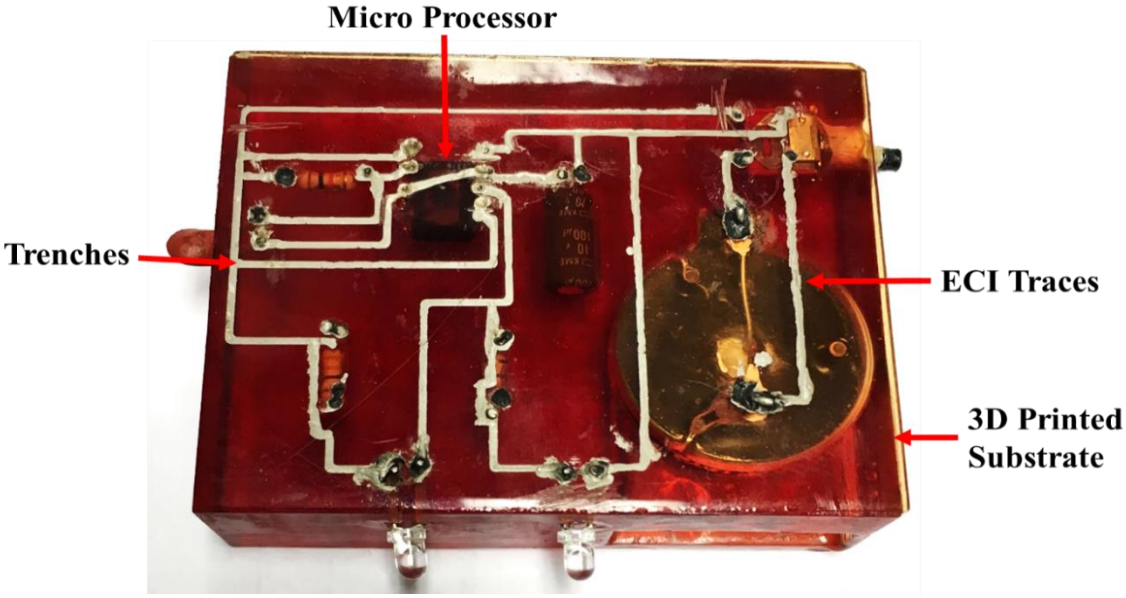

Figure 4. 3D printed multifunctional and structural electronics using ECI. White traces represent cured conductive ink that were dispensed in pre-specified trenches on a 3D printed substrate [18].

helps to dispense ink of specific dimension to the order of millimeter and flow rate to the order of milliliter per hour. The generation of predesigned and specific ink pattern on a substrate using an ink dispensing nozzle and computer controlled translation stage is known as direct write (DW). The combination of DW and AM created a platform to make structural and functional electronics. The authors in [18, 19], integrated AM and DW technology to fabricate structural electronics at W M Keck Center for 3D Innovation, University of Texas at El Paso (UTEP), USA. *Figure 4* represents the multifunctional and structural electronics fabricated by integrating AM and DW technology at W.M. Keck Center for 3D Innovation (UTEP).

Currently, the multi-functional additively manufactured components are fabricated using embedding or trenching process of conductive materials [15]. Progressive research works in the field of multifunctional 3D printed parts have attracted the relatively lower cost conductive ink, paste, and powdered materials in an electronics system. In [20-24], the authors provided the results for a relatively better understanding of the extrusion materials properties under thermal shock, vibration, tensile, and compressive load. The goal was to create the grading among silver particles contained conductive inks for functional electronics fabrication. The ultimate and key factor was the conductive materials that could increase the usefulness of the additively manufactured parts for multiple purposes. Investigation on the development of conductive path or curing behavior of those conductive materials in different environment such as in thermal vacuum environment will explore the opportunities of future fabrication and repair on outer space.

2.2 Direct writing technology

The ink dispensing technology advances with the progressive research work on conductive particles and organic binder of inks. According to the authors of [27-30], conductive inks can be deposited to create functional structured layers. This is defined as direct writing (DW). DW, three-dimensional printing (layer by layer) of conductive inks and other related approaches consist of patterning mechanism using a deposition head. *Figure 5* represents the classification of DW methods which are applicable to create a conductive trace and fabricate functional structures layer by layer. Authors in [31-34] described that the flow based direct writing technologies were involved in the deposition of liquid and colloidal conductive inks. Flow based conductive inks dispensing technique requires either a positive mechanical pressure device (syringe pump) or an extruder. Using these two devices ink deposition can be done in the following two approaches: (1) continuous trace and (b) droplet based. To obtain conductive trace on a substrate, continuous ink deposition is a reliable approach because it can create a conductive trace with specific trace

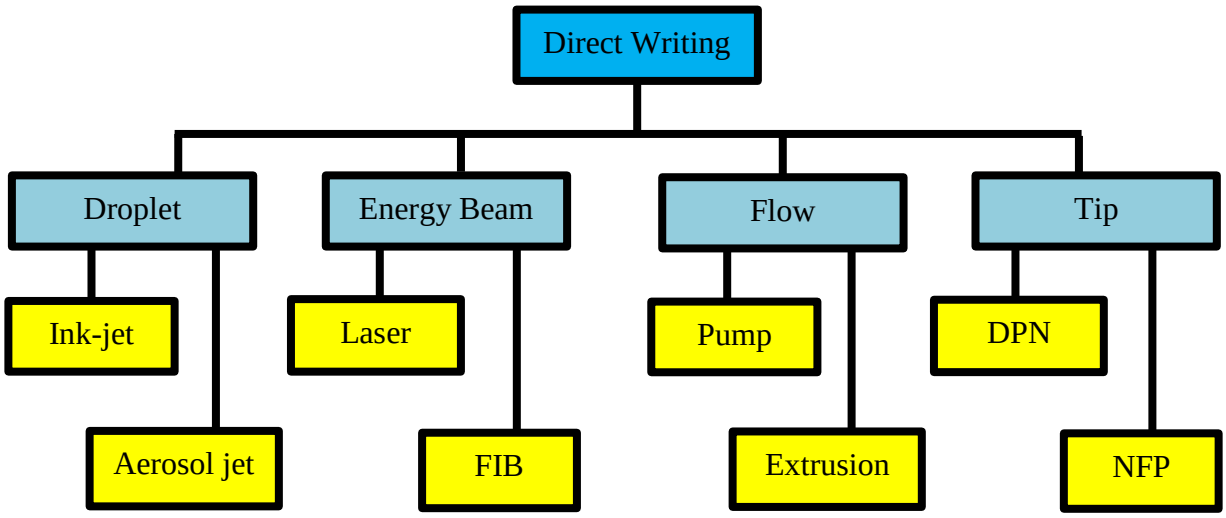

DPN: Direct pen nanolithography
NFP: Nanofountain pen
FIB: Focused ion beam

Figure 5: Classification of direct writing methods [33]

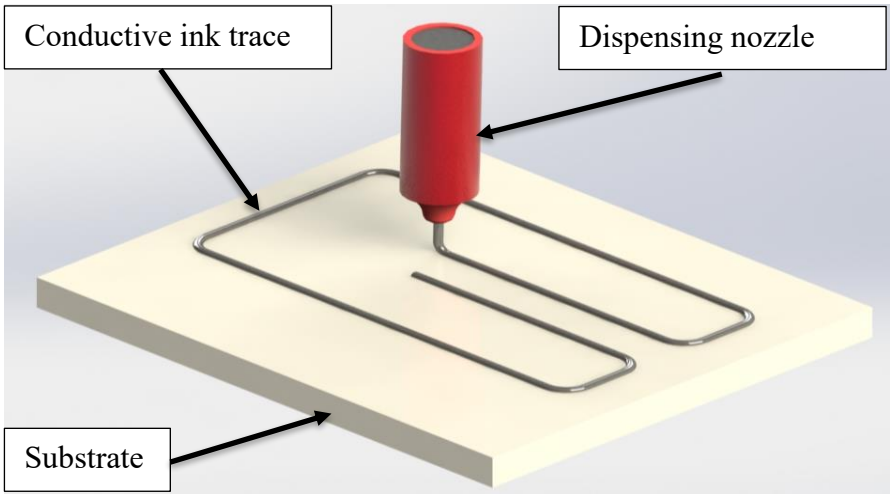

Figure 6: Schematic diagram of direct writing of conductive inks. Conductive inks are extruded directly on substrate during the movement of dispensing head.

dimension (micro meter to the millimeter). Commercially available small diameter ink deposition tips (e.g. 0.1mm to 1.5mm, Nordson EFD Inc.) are used to obtain a variety of trace in terms of thickness and width. Deposition tips are selected based on their trace dimension and the dispensing environment such as temperature, pressure etc. Figure 6 represents a typical DW system for conductive inks deposition on a substrate.

For continuous DW, dispensing valve and tips have been evolved through a tremendous effort in industrial and academic research and development. As a result, the three most well-known and established methods are known as nScrypt, MicroPen Technologies, and Nordson EFD Inc. (for the automated dispensing system). All of them are trademarks. The core technology of the nScrypt syringe based DW system is a high precision micro-dispensing pump with accurately controlled air pressure, timing, valve opening, and dispensing height [35]. MicroPen technologies for DW were produced by OhmCraft Inc. MicroPen technology uses an extrusion method to dispense conductive inks. It has unique writing parameters for each pen such as speed of writing, size of orifice, and deposition materials [36]. Using these available DW technologies, a hybrid

manufacturing platform was developed by authors of [18, 19] for structural electronics. They integrated the DW technology with additive manufacturing to fabricate functional and structural electronics. Similar technologies can be developed such as the DW on a 3D printed substrate or an existing electronic component (microstrip antenna, damaged solar array junction) to implement in space environment as a repair kit.

2.3 Conductive materials for DW technology

Most commonly used conductive inks in DW are silver (Ag) and copper (Cu) based. The formulation of metal based ink was investigated by changing the mixing approach of metal part and solution (alcohol or acetone). Those mixing approaches were investigated using both Ag based inks [14, 37-40] and Cu based inks [41-44]. The ability of a conductive ink to print and adhere to substrate depends on the ink formulation and composition e.g. conductive particles, polymer binder, and dispersant. Also, according to the authors of [26], the formulation mechanism such as selection and mixing of conductive particles and polymer solution dictates the conductivity property of the ink. The important rheological properties of inks are the surface tension and viscosity. The authors in [45], demonstrated that physical properties of the conductive ink trace relied on the viscosity, surface tension, and ink compositions as well. Conductive particles of ink try to accumulate together at a point on highly polished surface because it offers more surface tension on ink. A highly polished surface offers more surface tension on ink, which leads the conductive particles and polymer binder of the ink to accumulate together at a point [26]. Viscous ink tries to hold pre-specified trench on the substrate, although it requires higher injection force to dispense the ink. On the other hand, low viscous materials get the flattened pattern on the surface that is not desirable for printed electronics. To satisfy the demand of the printing in different

substrate materials, ink can be formulated in different ways. Table 2 represents a group of common ingredients of conductive inks.

There has been tremendous research done in creating conductive inks and colloids [27-40] that can be dispensed and cured to provide conductive traces. Jennifer A Lewis formulated a silver based conductive ink for that dimensional printing that has a highly conductive feature ($>10^4$ S/cm) at room temperature and atmospheric pressure [28]. All the steps involved in the silver ink formulation to the end user applications have been studied under room temperature and atmospheric pressure condition. Until now there is no such research effort found on the characterization of conductive inks in low pressure (less than 760 Torr) and low temperature (below 0°C). The author of this thesis is interested in using commercially available (previously studied at room temperature and atmospheric pressure) silver based DW conductive inks to characterize in low vacuum (10^{-2}Torr) and temperature range of -70°C to 70°C (representative simulated space environment). Using this characterization information, a DW repair kit can be developed for space application.

Table 2: Common Ingredients in Conductive Ink [45]

Ingredient	Desired function	Examples	Typical amount (wt %)
Electrical conductive filler	Conductive materials to develop conductive path	Metal: Silver, Copper, Nickel Metal precursor: copper oxide, nickel oxide, nanoparticles	10-60
Dispersing medium	Provides continuous phase	Non-polar solvent: tetradecane, ether, toluene,cyclohexane Polar solvent: water, ethanol, propanol, ethylene, glycol, diethylene glycol, glycerol, formamide,methyl ethyl ketone	30-70
Dispersant	Prevents fillers from aggregation	Polyvinylpyrrolidone (PVP), ammonium polyacrylate, sodium polyacrylate, anionic phosphated alkoxylated polymer (Solsperse 40), block copolymer with acidic affinity groups (Disperbyk 190), polycarboxylate ether (Sokalan HP 80)	2-10
Binder	Adhesion to the substrate	Organic binder: PVP, acrylic resin, vinyl acetate polymer, polyketone resin Inorganic binder: glass frits, borate nanoparticles, titanium and aluminium coupling agent	3-10

For vacuum applications, there are commercially available silicon RTV (Room-Temperature-Vulcanization) of diverse kinds (conductive, adhesive, nonconductive etc.). In [46, 47] the authors demonstrated that silicone has the low outgassing properties. Having the proved low outgassing value of silicone, they also formulated RTV materials for space application. All of the RTV materials were investigated at atmospheric conditions to determine the post curing physical and mechanical properties. Low outgassing test of cured RTV confirmed that silicone containing materials could be useful for space application. As a result, commercial organizations (Thorlab Inc., DuPont, Insulectro etc.) are claiming that they can produce space grade materials and parts needed to deploy in space or high thermal vacuum applications. Space grade materials

are used to protect the electronics components from harmful effects of UV irradiation, thermal shock, and the impact load of space debris. The challenging part to use the silicone RTV in space was to cure it at low temperatures and make a conductive path. Silicone based materials need the curing temperature to be above 100˚C, and the pressurized (more than 760 Torr) environment promotes the initiation of curing process as well. Since the materials with small amount of silicone (30% by weight) are less conductive and easy to pass the outgassing requirements, NASA was tried to mix some RTV materials, glass microballoons, silicone oil, a fumed silica (known as Cab-O-Sil) with a catalyst (amino propyl) triethoxy-silane (trade name A1100 under general electric subsidiary) to obtain the desired properties after curing in a simulated space condition [48]. Mixing of these elements and catalysts created a nonconductive trace to repair damaged part of space shuttle STS54 in the international space environment. It was cured in a space environment after 24 hours (vacuum condition) with the formation of some bubbles. Curing mechanism and bubble formation information in the experiment conducted by NASA and Lockheed Martin Corporation was helpful to study the feasibility of direct writing of conductive trace in space environment.

2.4 Development of conductive path on ink trace

The mechanisms involving in a conductive path development (or curing) dictates the application of conductive materials on electronics component fabrication. Materials are selected to print or manufacture of electronics parts based on the conductivity requirements and time to develop conductive paths. Therefore, it essential to understand the solidification process of ink traces.

From Table 2 it can be seen that there are several options available for a conductive ink formulation. The basic formulation of silver based conductive ink consists of two parts. Part one

is the silver particles that could be the flakes or nano particles. The second part is the solution that is nonreactive (inert) or reactive polymer binder.

Development of conductive path of a conductive ink with organic binders is shown in Figure 7. A conductive part in the form of flakes or nano-particles and a binder part in the form of an organic binder which is often a polymer. In solvent-based conductive inks, the organic part is a mixture of polymer and solvent. The curing process can be performed at room temperature or at

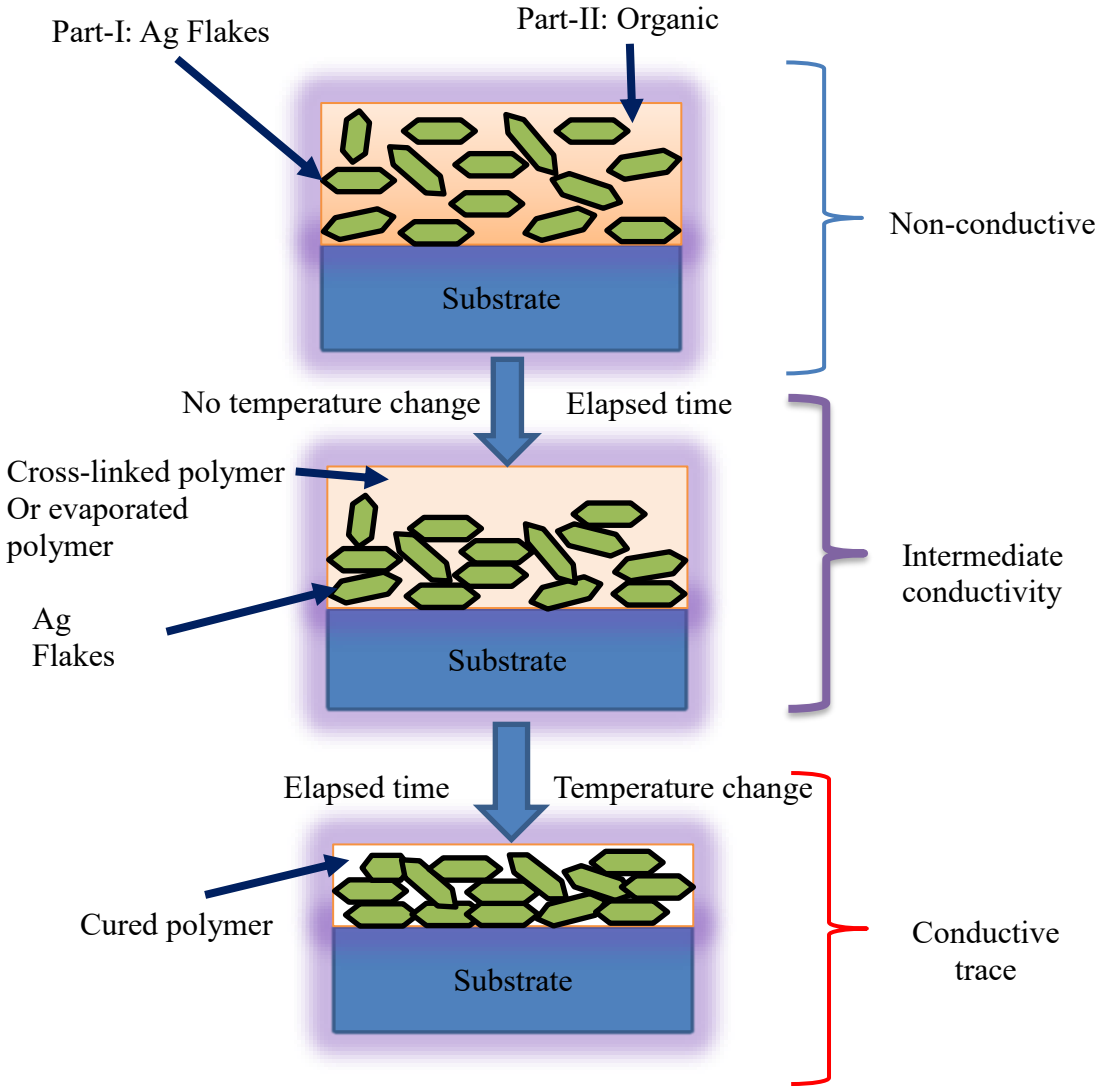

Figure 7: A flow diagram of the binding process of the Ag based conductive ink with elapsed time and change in temperature [29].

an elevated temperature. At room temperature curing, the solvent evaporates and the polymer starts to crosslink with elapsed time. Although curing at room temperature results in a conductive path via particle connections, there is increased the contact of particles when curing at temperatures above the debonding temperature. When the ink is cured at the debonding temperature, the polymer is removed from the matrix of conductive particles, which results in increased contact between the flakes [29].

The process of conductive path development depends on the system or environment pressure, temperature, degree of chemical reaction, and catalysts. Curing kinetics of conductive inks can be demonstrated by using the differential scanning calorimeter (DSC), thermo-gravity analysis (TGA), and scanning electron microscopy (SEM) etc. The analytical results also represent the mechanism of solvent evaporation and solidification. In DSC, a continuous supply of heat flow is needed to determine the initiation of curing time and total time required to completely cure the specimen. The measurement of heat flow in DSC is proportional to both the overall heat release and the curing rate as shown by the following equation [49]:

$$Rate\ of\ heat\ flow, \frac{dQ}{dt} = Q_r \frac{d\alpha}{dt} = Q_r k(T) f(a) \qquad \textit{Equation 1}$$

Where, $\frac{dQ}{dt}$ is the heat flow, Qr is the total heat released when an uncured material is brought to complete cure, $\frac{d\alpha}{dt}$ is the cure rate, α is the extent of cure, k(T) is the rate constant, T is the temperature, and f(α) is the reaction model. Rate constant of a reaction can be determined using the Arrhenius equation:

$$Cure\ rate, \frac{d\alpha}{dt} = A \exp\left(-\frac{E}{RT}\right) f(a) \qquad \textit{Equation 2}$$

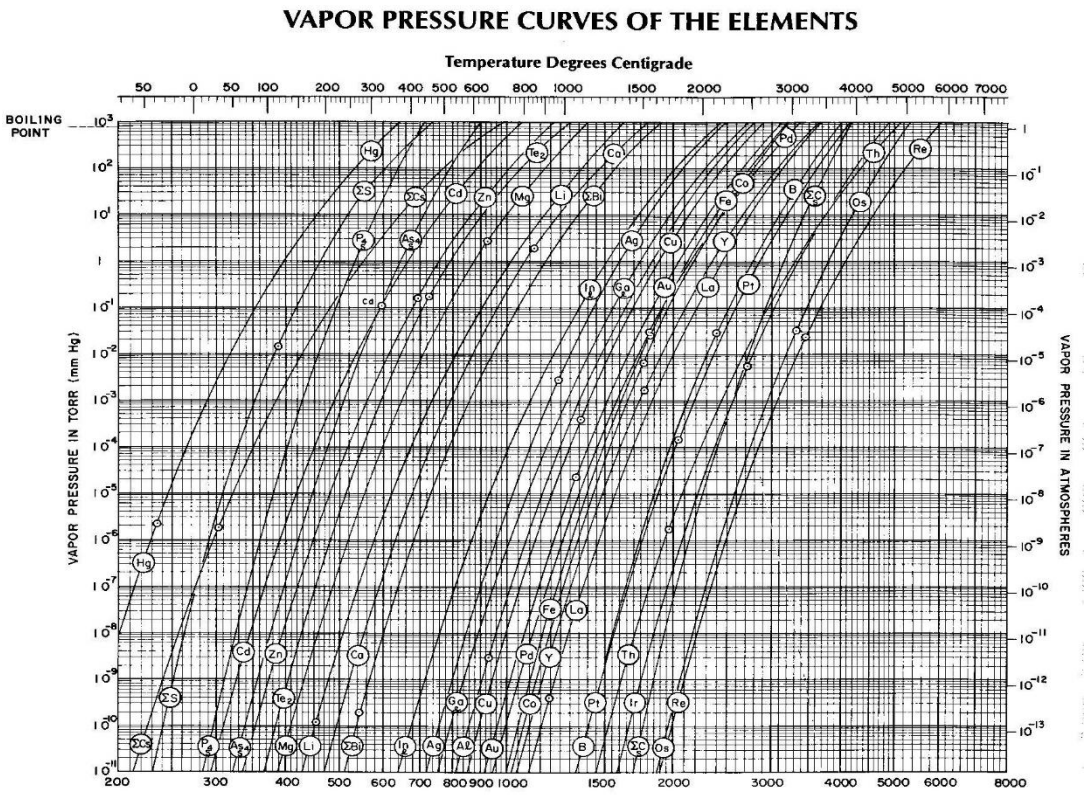

Figure 8: Temperature dependence of vapor pressure for the conductive elements i.e. metals of the periodic table. This graph informs about the vacuum pressure congenial to the evaporation of ink solvent from the bulk [50].

Where E is the activation energy of the reaction, A is the exponential factor, and R is the universal gas constant. By measuring the value of heat flow, temperature of the tested specimen and degree of reaction curing time can be determined graphically.

Additionally, the curing process depends on the vapor pressure and temperature of the material. Vacuum applicable materials need to satisfy the vapor pressure and temperature of the materials. *Figure 8* represents the vapor pressure graph of some common conductive elements used in ink preparation. The complete list of vapor pressure curve for the solid and liquid elements was developed by RE Honig and RCA [50].

The rate of evaporation under variable pressures and temperatures are key factors of curing in vacuum conditions. The initiation of evaporations of solution form the bulk depends on the vapor pressure and temperature. The rate of evaporation can be calculated using the following formula [51]:

$$Solvent\ evaporation\ rate\ (\%) = \frac{W_i - W_f}{W_s} x100 \qquad \textit{Equation 3}$$

Where, W_i is the weight of conductive materials before curing, W_f is the weight of conductive material after curing, and W_s is weight of the solvent in materials before curing. The rate of evaporation affects the curing process as the solvent evaporates and the conductive particles start to conduct electricity. Therefore, in vacuum or space environment, the development of a conductive path is different than the normal atmosphere.

The relation between vapor pressure and temperature of metallic ink can be described using the Clausius-Clapeyron equation. According to this equation, vapor pressure of the solvent of an ink is inversely proportional to the temperature [52]. *Equation 4* represents the relation between vapor pressure and temperature of a liquid ink.

$$\frac{dln(p)}{dT} = \frac{\Delta H_{vap}}{RT^2} \qquad \textit{Equation 4}$$

Where p is the vapor pressure of the liquid, T is the temperature, H_{vap} is the enthalpy of vaporization and R is the universal gas constant.

Shelf life and operational life of an ink are important for DW of printed electronics applications. Premature solidification creates the clogging in dispenser orifice and prevents the injection on the substrate. The authors in [45, 53, 54] described the methods to modify the shelf life of conductive inks. According to their guideline of ink formulation, the filler or conductive particles of inks should be less than one-hundredth of the nozzle diameter. Also, the dispersant is

an essential part of conductive inks that dictates the shelf life. These criteria are helpful to select the inks for a particular application as well as to determine the shelf life. This thesis deals with the metallic conductive inks such as silver particles based inks. This is because silver based conductive inks have the potential to be dispensed and cured at low vacuum pressure as well as in a wide range of temperatures (45℃ to 150℃). Using the previous research information and manufacturer data sheet on curing of silver based conductive inks, the author proposed to develop a repair kit that creates a conductive trace using DW technology in space environment.

2.5 Space environment

In the space environment, there are some complications such as damage to surfaces and subsurface materials of components due to the space hazards. According to the authors of [1, 12, and 55], the space environment consists of hazards such as space debris, ultraviolet radiation, plasma etc. 'Space hazards' name came due to their antagonistic effects in comparison to earth environment. *Figure 9* represents some common space hazards elements. Although to create a simulated space environment all the space hazards need to be incorporated in a vacuum chamber, the author focused on the low vacuum pressure and temperature only. This thesis is helpful for the future experimental investigation, that will integrate all kinds of space hazards in a thermal vacuum chamber.

Figure 9: Common hazards in space environment [49]

The vacuum in the space environment means the pressure below the atmospheric pressure (1 atm =14.6 psi or 720 Torr). There are different levels of pressures in different orbits and altitudes. For experimental purposes to simulate the space environment in a laboratory, vacuum levels are classified according to the pressure ranges of different orbits and altitudes. Table 3 represents the different vacuum levels used to simulate the space environment in a laboratory.

There are some advantages and disadvantages of a vacuum environment. The advantages of a vacuum environment can be seen in chemical vapor deposition and microstructural image acquisition technology, etc. By removing the foreign and unwanted gaseous molecules from a closed chamber, pure substrate can be deposited or topographical image can be achieved. On the other hand, a vacuum has some hazardous effects in space. In summary, the following three potential problems can be created due to vacuum in space. First, a thermal vacuum creates the outgassing of trapped molecules from surface and subsurface of the materials. Outgassing of materials degrades the material and shortens life spans. To meet the NASA low outgassing requirements, spacecraft materials should comply with either ASTM E1559 [56] or ASTM E595 [57] test. Secondly, cold welding is another potential risk of the thermal vacuum. Two metallic parts are fused together due to the cold-welding effect in space so there is a probability of locking any mechanism and having it clogged forever. Third, in a vacuum environment (below 0.1 Torr)

Table 3: Vacuum level classification

Classification	Vacuum level (Torr)
Low vacuum	1 to 10^{-3}
Medium vacuum	Less than 10^{-3} to 10^{-5}
High vacuum	Less than 10^{-5} to 10^{-8}
Ultra-high vacuum	Less than 10^{-8} to 10^{-12}

there is only one heat transfer mode active, which is radiation heat transfer from source to sink [55].

Temperature variation is common phenomena in the space environment. At sunlight condition, temperature can rise to 150˚C, and no at no sunlight temperature can fall down below -150 ˚C depending on the orbit and altitude. The coefficient of thermal expansion (CTE) is a thermodynamic property that depends on the temperature of the body and surrounding environment of materials. Since it is thermodynamic property, it depends on the temperature change. At low temperature (-73°C), a specific material such as stainless-steel (304) shrinks (14.8×10^{-6} mm/mm.℃) and at high temperature (205°C) it expands (16.6×10^{-6} mm/mm.℃). Although this study did not evaluate CTE of conductive inks, a description is important in space environment is offered to demonstrate the change in dimension of parts due to temperature change. Following calculation provides an idea about the effect of temperature change in length of a stainless steel (304) part.

Assuming, at room temperature (T_0=23℃) a stainless steel bar has a length (L_0) 100mm. The coefficient of thermal expansion (α) of stainless steel bar is 17.3μm/m.℃. Due to the increase of temperature (T_f) to 100℃ changes of length (ΔL) can be calculated using *Equation 5*: [58]

$$\frac{\Delta L}{L_0} = \alpha \times (T_f - T_0) \qquad \textit{Equation 5}$$

$$\Delta \mathrm{L} = L_0 \times \alpha \times (T_f - T_0)$$

$$\Delta \mathrm{L} = 0.100 \times 17.3 \times 10^{-6} \times (100 - 23)$$

$$\Delta \mathrm{L} = 0.16781 \text{ mm}$$

From above calculation, it obvious that length of stainless steel bar was changed due to the temperature change. Therefore, if any mechanisms or systems have two or more different materials with different CTE, then it is necessary to consider the temperature change effect on design because temperature change will create the dimensional inaccuracy, which may lead the failure of any component. Hence, the material's coefficient of thermal expansion (CTE) is an important factor for space applicable materials within the wide range of thermal cycle (-150℃ to 150℃). The sudden variation of temperatures in space can be predicted according to the altitude and pressure as of orbital function. A standard rule of thumb was fixed by NASA for the thermal cycle to test any materials between -120˚C to120 ˚C [59].

The authors in [60] described that the natural space radiation environment can be classified in two groups: i) particles trapped in planetary magnetospheres or belts including protons, electrons, and heavier ions, ii) transient particles which include galactic cosmic ray particles such as protons and heavy ions of all the elements of the periodic table. Solar events such as coronal mass ejections flares are also included in the transient particles. The radiation belt in space environment has two parts. The belts are donut shape as shown in Figure 10. The inner part of the belt (extended between 400 km to 18,400 km from the earth's surface) is known as Van Allen Probe-A. It consists of electrons and energy density is 10 MeV. The outer part is known as Van Allen Probe-B (20,000 km above the earth's surface). It consists of proton fluxes with energy density greater than 30MeV [60]. The radiation environment with these band of energies causes

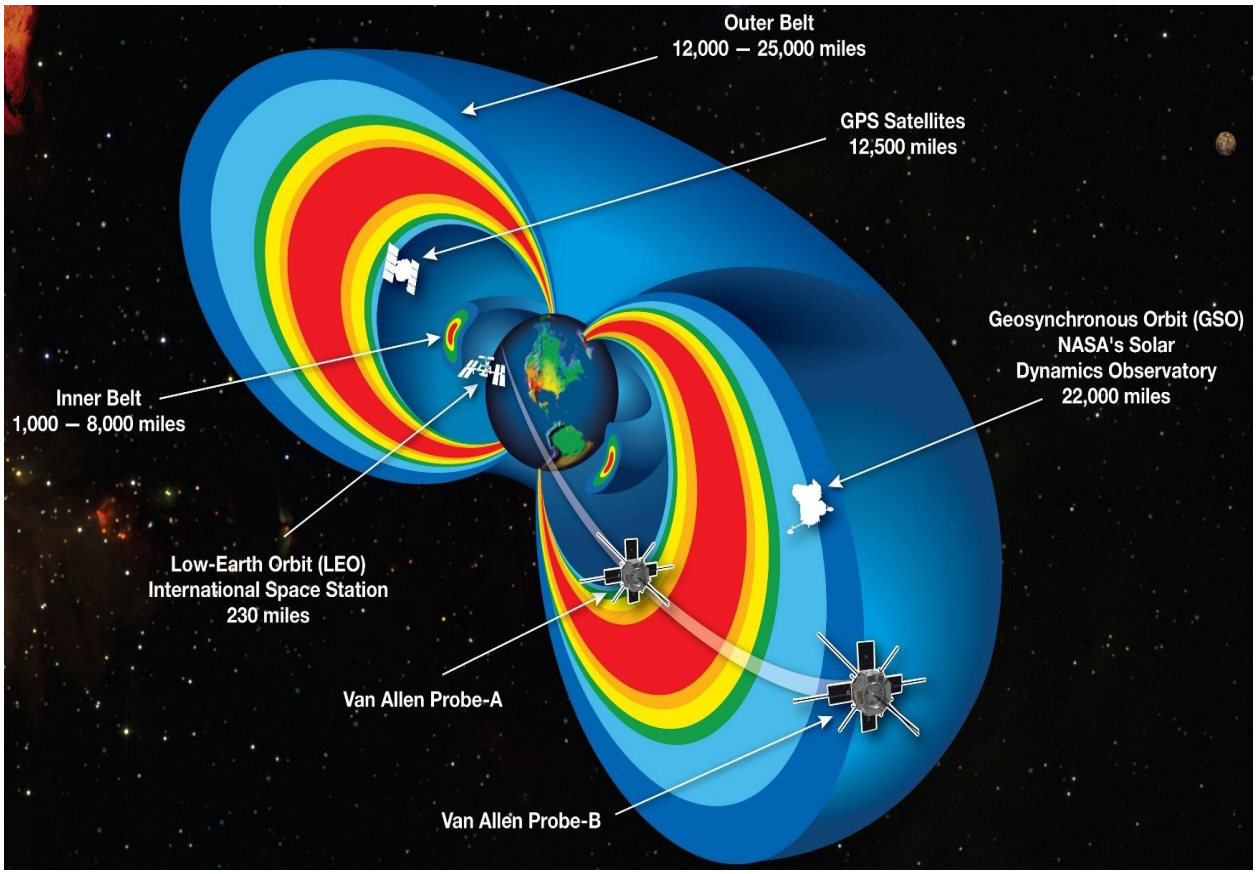

Figure 10: Natural radiation belts in space environment [61].

detrimental effects on material surface and subsurface. In short, the radiation environment in space can lead to following potential issues on a spacecraft: i) heat generation, (ii) degradation and damage of electronic components such as antenna, solar array junction and, [iii] creation of solar pressure that is exerted by electromagnetic radiation wave of sun light [55, 62, 63].

The plasma which is known as the fourth state of matter, in the space environment is approximately equal to the amounts of positively charged ions and negatively charged ions or electrons. Plasma density differs with respect to the solar radiation and altitude. Closer contact of charged particles, which comes from either solar radiation or Van Allen belt to the materials in the space environment, may cause the harmful impact by building up the negatively charged surface.

Sputtering, arching and single event phenomenon are the potential risks of the plasma environment [55, 59].

According to the authors of [1, 55], the space environment has a significant amount of debris and micrometeoroids. Front faces of a space shuttle are most likely impacted by the micrometeoroids whereas the back side or ram has the less chance to collide with the moving debris. The impact of debris depends on the size and velocity of a vehicle during the strike. Obviously bigger debris will create or initiate the crack in a bigger scale, but the small debris or micrometeoroids can also create the harmful impact by introducing the stress and strain in molecular levels. In the ground testing facility, some hydrodynamic testing can predict the failure criteria of micrometeoroids impact, but for larger debris impact there are limited scopes of testing of the materials or entire structures [55]. In the space environment materials are prone to fail with minimum impact as compared to the ground testing because the trapped molecules evaporate from surface and subsurface and create gaps between solid particles. Meanwhile, the electrostatic force and temperature gradient (low temperature or high temperature depending on the dark and sunlight condition) weaken the bonding of solid particles in materials. Therefore, to maintain the specific requirements of space applicable materials, certain measures (low outgassing, thermal cycling etc.) need to be taken during the materials failure criteria. Each mission is also accumulating the space debris by losing the parts of spacecraft or degrading the older parts of a satellite. Hence there is a probability that the future space vehicles and satellites will be affected by that man-made debris.

The authors in [59], reported that in space environment the gravity is not absolute zero. The gravitational force depends on the distance and, as the object moves further away, gravitational force decreases. A low gravity condition is known as the free fall. In low earth orbit, there is 91% of gravitational force existing as it is on the earth's surface. Therefore, the gravitational force never

goes to absolute zero. During the space craft design, the mass of the vehicle is considered in such a way that in the space environment, less gravitational force can affect the velocity of the vehicle. In manufacturing or fabrication point of view, low gravity has an advantage for uniformity of the internal structure. At low gravity, elementary particles are distributed uniformly over the substrate's surface which is always desirable. The difficulty arises when there is less adhesion force existed between two materials. For a liquid that made a concern among engineers mostly, the splashing or splattering occurs in free fall condition that ultimately hampered the manufacturing in vacuum environment (space condition). Therefore, a gravitational force or relatively higher adhesion force is needed to overcome the splashing phenomena.

The space environments (space hazards) are always unfriendly for any parts fabricated in atmospheric conditions, because the temperature fluctuations, vacuum, and space debris degrade the physical and chemical property of materials [62-64]. Therefore, some requirements need to maintain such as low outgassing (collected volatile condensed mass (CVCM) less than 0.1% or the total mass loss is less than 1%) during materials selection and manufacturing process in space environment. Materials selection for space application depends upon the materials physical and chemical properties. Low outgassing (ASTM E595) and degradability (ASTM E1559) tests are commonly used for selecting space grade materials [56, 57]. Both tests determine the collected volatile condensed mass (CVCM), total mass loss (TML), and water vapor regain (WVR) value after vacuum testing (24hrs cycle test). Parts fabricated using subtractive or additive manufacturing often undergo post manufacturing operations that are needed to cure and improve the physical properties such as mechanical, thermal, electrical, morphological, and operational lifespan.

Chapter 3: Methods and Experiment

This section will describe the design and fabrication of a mechanism for dispensing conductive inks in space conditions. In addition, characterization (i.e., continuity and scanning electron microscopy) of the ink behavior was tested in the following conditions:

- atmospheric conditions (temperature 25˚C and pressure 760 Torr)
- low temperature (T = -50˚C), atmospheric pressure (P =760Torr)
- high temperature (T = 80˚C), atmospheric pressure (P =760Torr)
- low temperature (T = -50˚C), vacuum pressure (P = 0.01 Torr)
- high temperature (T = 80˚C), vacuum pressure (P = 0.01 Torr)

A continuity test is a method to determine whether a circuit is open or closed to conduct electricity. When the circuit is open there is no flow of electricity. The closed circuit allows current to flow, which is known as the continuity. A continuity test cannot provide any information on path resistance but only that path can carry electrons. This thesis uses the techniques of continuity test to determine the time required to develop a conductive path in the ink traces under different environmental conditions such as low temperature (below -20℃), high temperature (70℃), atmospheric pressure (760 Torr), and vacuum pressure (10^{-2}Torr). The combination of voltage divider rule and continuity test principle was used to determine the current flow across the conductive trace of inks. For each test, total supplied current was 0.9 to 1mA. According to voltage divider rule, the current was divided into two specimens by 0.5mA. During the experiment, maximum current flow through each specimen was 0.3mA. According to Ohm's law, current flow through a conductive trace is proportional to the voltage difference.

$$V = IR \qquad \textit{Equation 6}$$

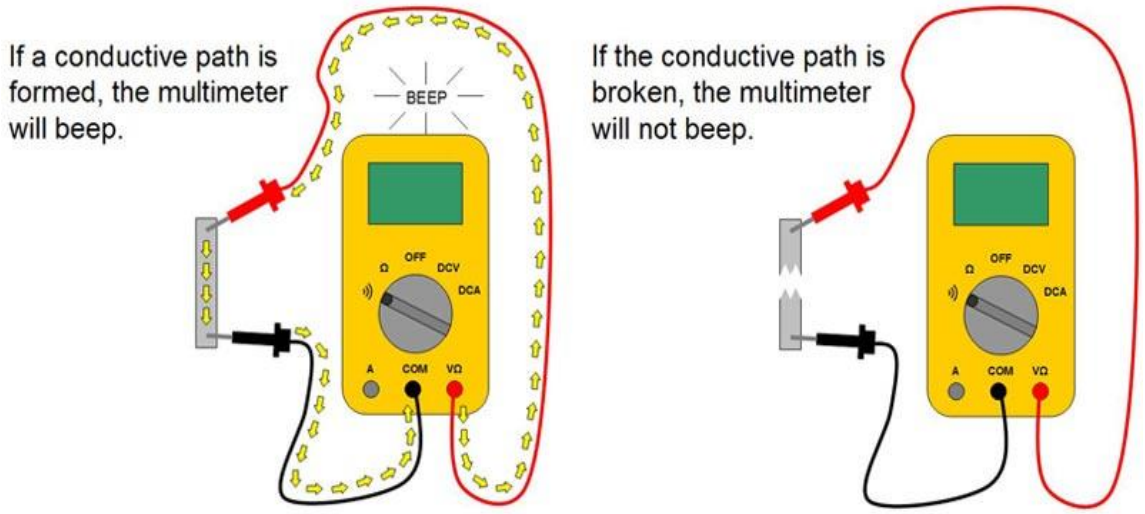

Figure 11: Schematic diagram of the continuity test principle the figure on the left demonstrates a closed circuit, and the figure on the right demonstrates a broken (open) circuit.

Where V is the voltage drop across the ink trace, I is the current flow through the ink trace, and R is the resistance of the ink trace. For the open circuit, resistance (R) value is infinite and for a closed-circuit resistance has a finite value. By knowing the value of resistance and current flow, the voltage drop can be calculated. Otherwise, from voltage drop and current flow, resistance can be measured using Ohm's law. The simplest method is to use a digital multi-meter to determine if the circuit is open or closed. *Figure 11* demonstrates the continuity test of a conductive block. When the circuit is closed, the multimeter will indicate continuity either by sound (i.e. a beeping sound) or a visual indicator.

To measure the initiation of conductivity time and characterize the conductive behavior of inks, several experimental techniques are available. In [66], the authors used differential scanning calorimetry and thermo gravity analysis to investigate the curing time for the epoxy-based conductive adhesive. In [67], the authors used the elevated temperature curing, which was named as ohmic curing. Also, the microstructural characterizations by SEM were done to analyze the

necking phenomena of cured and damaged silver particles in conductive ink. Laser curing is mostly used for rapid curing of conductive ink. The authors, in [68] described the curing process using UV light generated by a laser and characterized the curing process of conductive ink. However, none of the above-mentioned curing processes were done in the space environment or similar conditioned environment to investigate the conductive path development process. This research introduced a new and simple method to measure the initiation of current flow after ink dispensing in a representative space environment. In addition, the total time required to obtain the maximum current flow of the conductive inks were measured and made a ranking of potential application in future space DW.

In liquid form, the electrical conductivity of the ink is zero because there is no current flow across the ink trace or film. When the temperature of the ink increases, cross-linking and evaporation of liquid solution leads the process of building a conductive path on ink (process has been described in Figure 7). Since the conductive path development is a temperature and time dependent process, the characterization is also defined according to the required time of maximum current flow through the conductive ink trace and temperature. To investigate the conductive path development process, all the experiments were conducted using a similar concept of a continuity

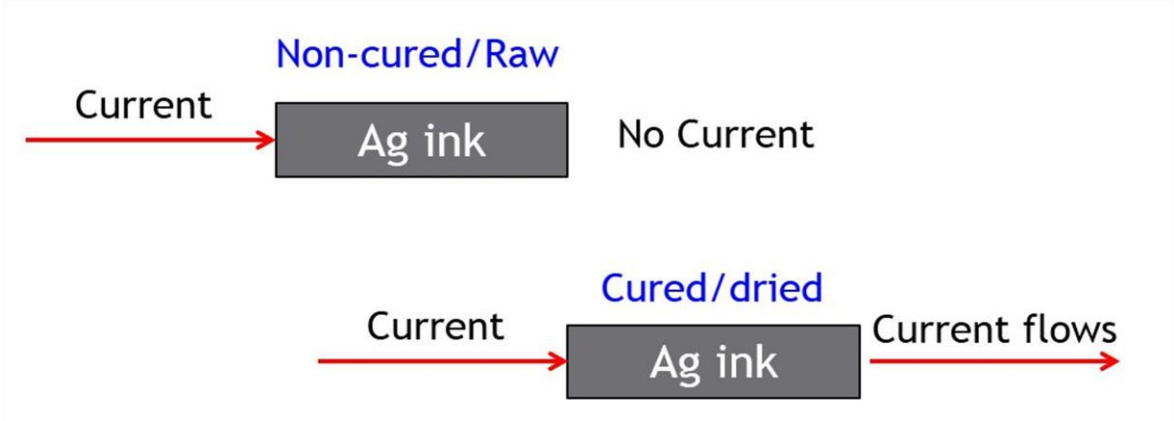

Figure 12: Representation of conductive property of a liquid ink before and after developing conductive path.

test. A similar methodology can be employed to determine the curing time and resistance of the trace of the ECI as shown in Figure 12. When the ink is liquid there is no current flow, which refers to that circuit is open. As the ink starts to cure it enables current flow. A cured ink gives the approximately same amount of voltage and current that is provided from the power supply unit. The total resistance of the printed trace can be calculated by determining the value of voltage and current flow across the trace.

The discussed test procedure was employed in both thermal vacuum system and atmospheric thermal environment testing. Only the sample test bed was placed inside the chamber and rest of the element such as the power supply, data acquisition system etc. was placed outside of the chamber.

3.1 Materials

Previously studied and tested for DW application, two different types of conductive inks were selected for the experimental investigation. Both inks were silver based conductive inks but the particle sizes were different. The Ercon E1660 (Ercon Incorporated, Wareham, MA USA) is a micro particle-based which has the flakes of silver (20μm). It's controlled electrical properties such as dimensional accuracy in trace and uniform liquidity during injection, are useful for many applications including electrical terminators, printed circuitry, sensor leads, printed antenna etc. [69]. The other tested conductive material was DuPont CB102 (DuPont Microcircuit Materials, Research Triangle Park, NC 27709) conductive paste [70]. Both materials have some unique properties which are looked-for the possible application in space. Though they have a significant difference in some property, for instance, they have equivalent resistivity (*Table 4*), but the

viscosities are different. CB102 silver nanoparticle conductive ink was selected for testing, because of its low outgassing performance, which is required for space applications. CB102 has a total mass loss 0.059% as determined by ASTM E595. The CB102 outgassing performance is below the 1.0% of NASA requirements. Also, the collected volatile condensable material is 0.026%, which is less than the maximum NASA acceptable value 0.10%. The challenges of the CB102 are the shelf life (less than 3 months) and storage temperature (below 5˚C). Adding ethanol by mass ratio with CB102 increases the shelf life and reduces the viscosity. In experiments described in this manuscript, the addition of ethanol was done only to reduce the viscosity.

According to manufacturer report, E1660 silver flake based conductive inks have the shelf life of 6 months at room temperature (22˚C). It has the viscosity of 17. 5Pa.s, that is favorable for flow based direct writing technology and three-dimensional printing. Controlled trace thickness (as there was no swelling or expansion after dispensing) and a short time to conduct electricity (approximately 1 to 5 minutes) at an elevated temperature increased the curiosity for experimental study in vacuum condition. Until recently, there is no information about the space application of E1660. For the experimental studies, other materials (CB100, CB028) were chosen, but some

Table 4: Conductive materials properties [49, 50].

Materials	Viscosity (Pa.s)	Bulk Resistivity (Ω/cm^3)	Physical appearance	Silver Particles Size (μm)	Structure of Particles	Curing Time at Atmosphere
Ercon E1660	17.5	2.1×10^{-4}	Silvery	20	Flake	1-5 Minutes for 121˚C
DuPont CB102	85	1.8×10^{-4}	Bright Silvery	1-5	Nano	60 Minutes for 150 ˚C

Table 5: Low outgassing properties of ULTEM 9085 and Proto Therm 12120 [72].

Material	CVCM (%)	TML (%)	WVR (%)	Total = TML-WVR (%)
ULTEM 9085	0.00	0.04	0.32	0.28
ProtoTherm 12120	0.01	0.71	0.20	0.51

CVCM: Collected Volatile Condensable Mass (if ≤ 0.1%, then space applicable or if TML-WVR ≤ 1.0%)
TML: Total Mass Loss
WVR: Water Vapor Release

initial parameter such as high CVCM (greater than 0.1%), low vapor pressure (7.5 Torr) of the polymer solution within inks eliminated them from further testing.

3.2 Micro dispenser design and printing

To inject the ECI, a micro dispenser was modeled and printed using stereolithography (SL printing) as shown in *Figure 13*. The dispenser (injector) contains a spring-loaded valve and a spring-loaded piston within the injector. The spring inside the injector is compressed and exerted a force on the piston to inject the ink. Another spring was used to create a normally-closed (NC) valve at the tip of the injector. To open the NC valve, a burn wire (30 AWG type Chromel C) mechanism released the compressed spring, to inject the conductive ink. In [71], the authors used the burn wire mechanism, because it is allowable in space applications and more reliable than other valve mechanisms such as solenoid valve, screw thread or stepper motor related mechanism. For small 1U CubeSat, power and mass budget always limits the capability of advanced mechanism in large scale. Therefore, lightweight and a simple mechanism such as burn wire release mechanism is popular for space application. The dispenser is supported by the rail support and carriage. Two stainless steel rods were used to guide the dispenser. A threaded rod, coupled with a stepper motor

(AM1020-ww-ee, MICROMO, 14881 Evergreen Ave., Clearwater FL 33762) was used to drive the dispenser for 40mm length.

The leaking of ink at the injector's tip was a challenge. Two space grade O-rings were used along with the NC valve for sealing purposes. Though the injector was 3D printed to dispense the ink in space environment, a conventional 10ml luer-lock syringe (BD, Franklin Lakes, NJ) was used for testing of ECI in the thermal laboratory environment. The conventional syringe was equipped with a Nordson EFD precision dispensing tip (Nordson EFD, Providence, RI), whose orifice diameter was 1mm.

For the space application, ULTEM 9085 or ProtoTherm materials need to be used. These two materials have low outgassing (less than 0.1% CVCM) properties and required mechanical, physical and thermal properties to survive in space environment. *Table 5* represents some important low outgassing properties for ULTEM 9085 and ProtoTherm materials for space application. ULTEM 9085 was not used because the fused deposition modeling or FDM technology has the limitation on the resolution as compared to the SL printing. It is expected that

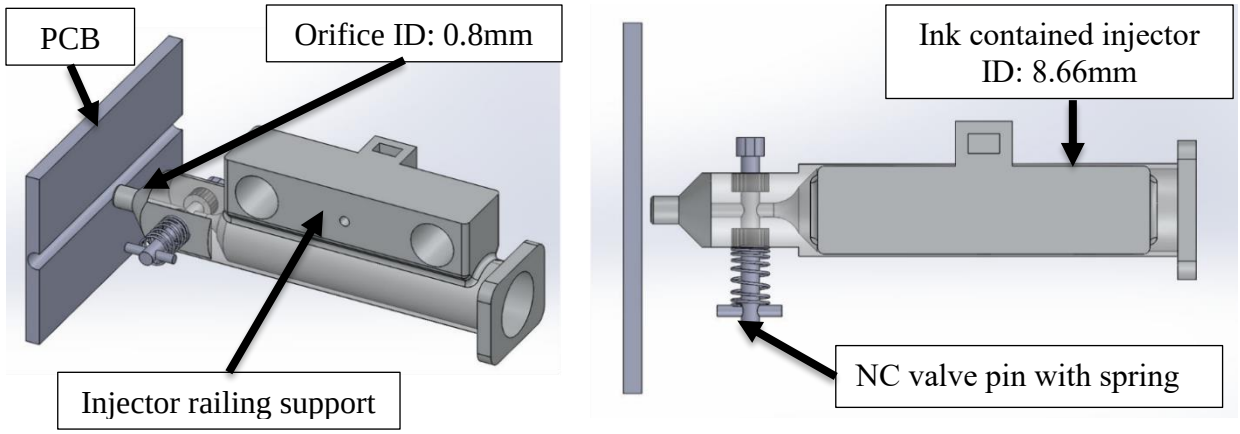

Figure 13: Assembled CAD model of the Micro ink dispenser system showing the major components such as the 3D printed ECI substrate where the ink is dispensed, injector railing support to control print head movement and normally closed (NC) spring loaded valve that controlled the orifice.

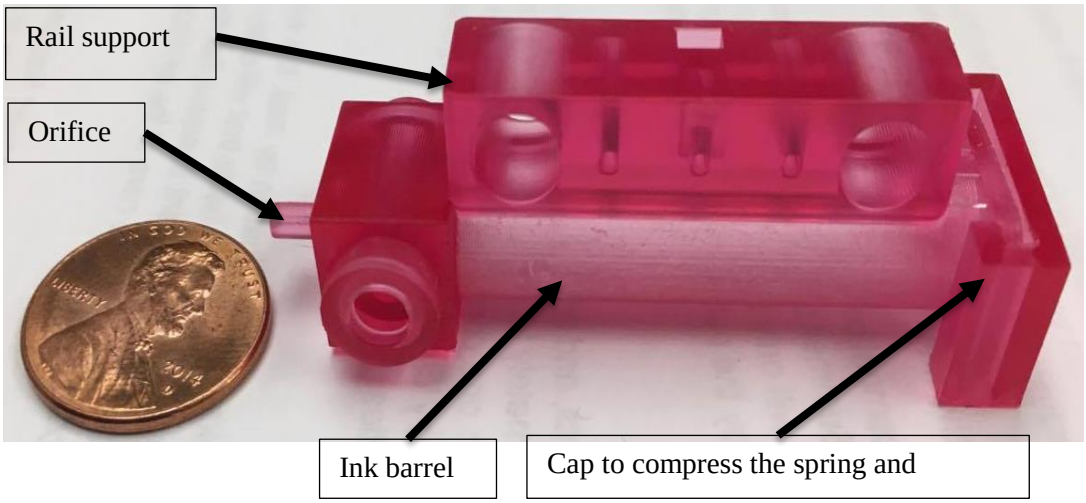

Figure 14: A SL printed (ProtoTherm) functional prototype of the micro dispenser. Length of the dispenser is 65mm, inside diameter of the ink barrel 8.66mm.

surface roughness of FDM parts is 70% larger of a SL part, so the friction force will also be larger. Therefore, an injector was printed using ProtoTherm material (SL printed part) as shown in *Figure 14*.

3.3 Spring selection and test

As the microdispenser for 1U CubeSat payload was spring loaded, a space grade stainless steel spring was selected. In the thermal environment, the extension spring can degrade the mechanical properties. In [73], the authors investigated the spring constant at thermal cycle. Results of the investigation indicated that extension spring constant reduced at low temperature and high temperature environment. Since there was no information about the compression spring

degradation in thermal environment, therefore investigation on spring constant variation in thermal environment was required. For the experiment of compression spring constant variation in thermal environment, stainless steel spring was chosen (*Figure 15*). Properties of this spring can be found in *Table 6*.

Using the Hagen–Poiseuille equation (*Equation 9*), the minimum force required to inject the ink from dispenser was calculated at 10.02N.

$$\text{Pressure drop in barrel due to viscosity } = \frac{8\eta l Q}{\pi R^4} \qquad \text{Equation 7}$$

$$\text{Viscous resistive force } = \frac{8\eta l_n Q R_b^2}{\pi R_n^4} \qquad \text{Equation 8}$$

Total injective force is the summation of viscous force and the friction force between plunger and injector wall. Therefore,

$$Injective\ force = \frac{8\eta l_n Q R_b^2}{\pi R_n^4} + plunger\ friction\ force \qquad \text{Equation 9}$$

In this equation, flow rate, Q = 5ml/min, length of the injector, l = 75mm, length of the orifice l_n = 6mm, radius of the injector R_b = 4.33mm, radius of the orifice R_n= 0.4mm, viscosity of ink η = 18.78 Pa.s. The frictional force between the plunger and injector wall was determined

Table 6: Properties of the compression spring used for the injector to inject ink.

Property	Overall length, mm (in.)	Outer diameter, mm (in.)	Internal diameter, mm (in.)	Wire diameter, mm (in.)	Compressed length, mm (in.)	Maximum load, N	Spring constant, N/mm (lbs/in)
Value	38.1 (1.5)	7.95 (0.313)	6.17 (0.243)	0.88 (0.035)	22 (0.867)	17.7 (3.98)	1.36 (7.76)

by Instron the tensile testing machine. By calculating the viscous force and friction force, total force required to inject the ink was determined which was 10.02N. Therefore, a stainless-steel compression spring was selected according to the required injective force.

The intention of spring testing was to determine whether the spring can provide the minimum force in low temperature and high temperature condition. The spring test was performed using Instron tensile testing machine. Details of the tensile testing machine and its thermal

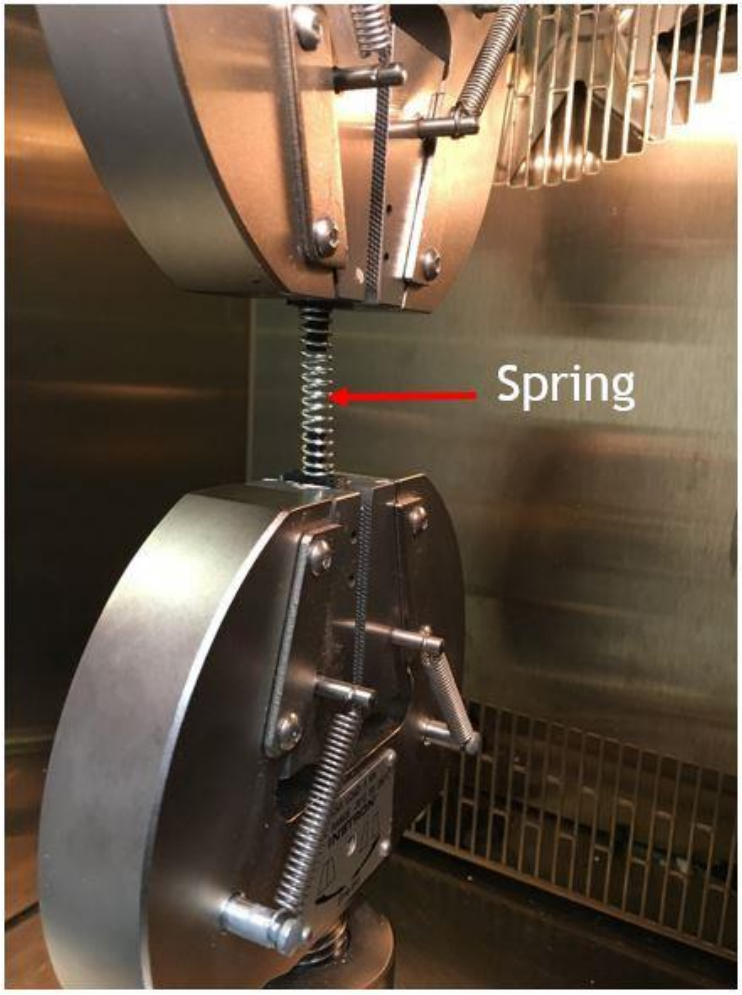

Figure 15: Testing of variation of spring constant of spring at Instron tensile testing machine under thermal cycle. Temperature range of the testing was -50˚C to 80˚C using LN2 flow and heater in environment chamber.

environment discussed in later thermal testing section. The crosshead was moved at a rate of 5mm/min. Data were collected to construct force vs compression length graphs, from which a spring constant at a specific temperature was determined. Separate tests were performed at -50°C, 22°C, and 80°C.

3.4 Test sample preparation

A printed circuit board (PCB) was chosen as a substrate to dispense the ECI. The test PCB as shown in *Figure 16*, was manufactured using CNC machine. The first step was to create a CAD design of a set of connection paths on PCB. Then, the CAD file used to create Gcode for the CNC machine to remove the copper and create the open path of the continuity test circuit. To mitigate risk in the case that the printed trace failed during deposition, two circuitry paths were made on the PCB. The distance between the two connections that was filled by the ECI trace was 7mm. Overall PCB dimension is 50mm×35mm. All wires external to the PCB were connected to the copper foil paths by using solder. Bulk layer (the layer between the top and bottom copper

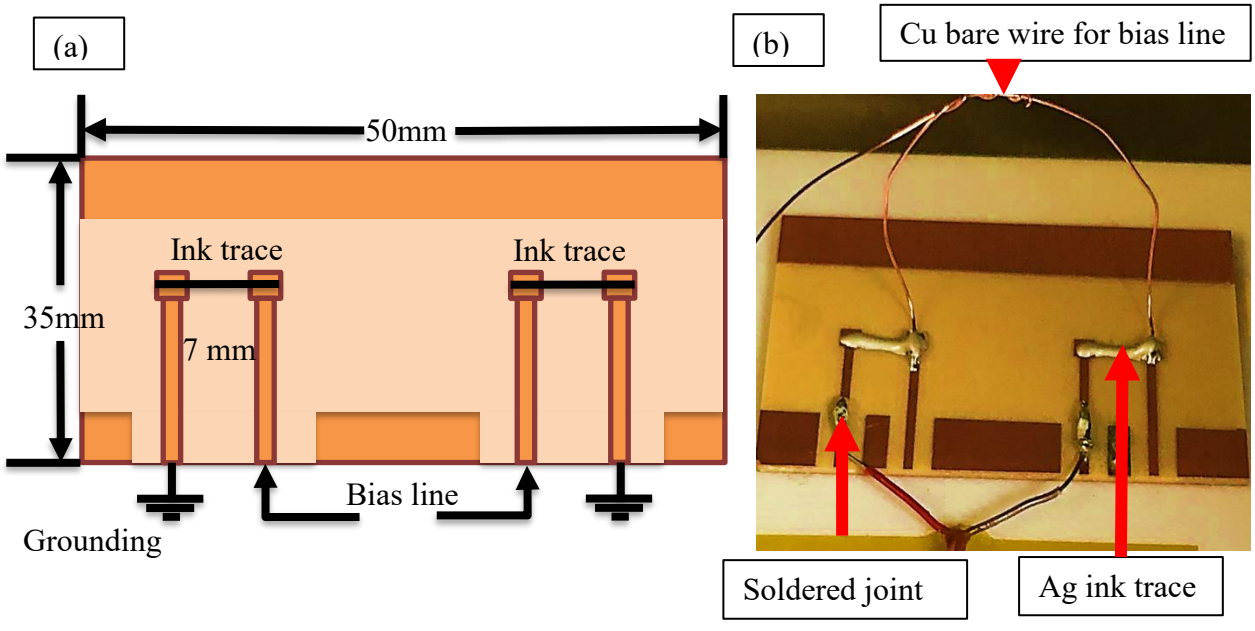

Figure 16: (a) Schematic diagram of PCB (b) Manufactured PCB for ECI testing.

cladding) of the PCB was electrically insulated but thermally conductive. Conductor layer helps to radiate heat in surrounding environment. The reason for removing the copper cladding was to make the PCB surface an electrical insulator and thermal conductor.

To determine the temperature of the ink and substrate, two thermocouples were placed on the plastic part of the PCB which is shown in *Figure 17*. An ABS plate (15cm×13cm×2cm) which was made by 3D printing, used to create the isolation between the base of thermal chamber and PCB. The bare part of the electrical wire and thermocouple sensor was covered by the Kapton® Polyimide tape. Gaseous particle inside the chamber might accumulate on the bare wire and thermocouple sensor resulting in faulty conductance results. Therefore, the bare wire was covered with Kapton tape before running the test. Also, thermocouple sensor was covered with Kapton tape and followed by the aluminum tape was used in order to adhere to the PCB board. The aluminum tape was used to adhere the Kapton tape on the PCB board. Because at low temperature

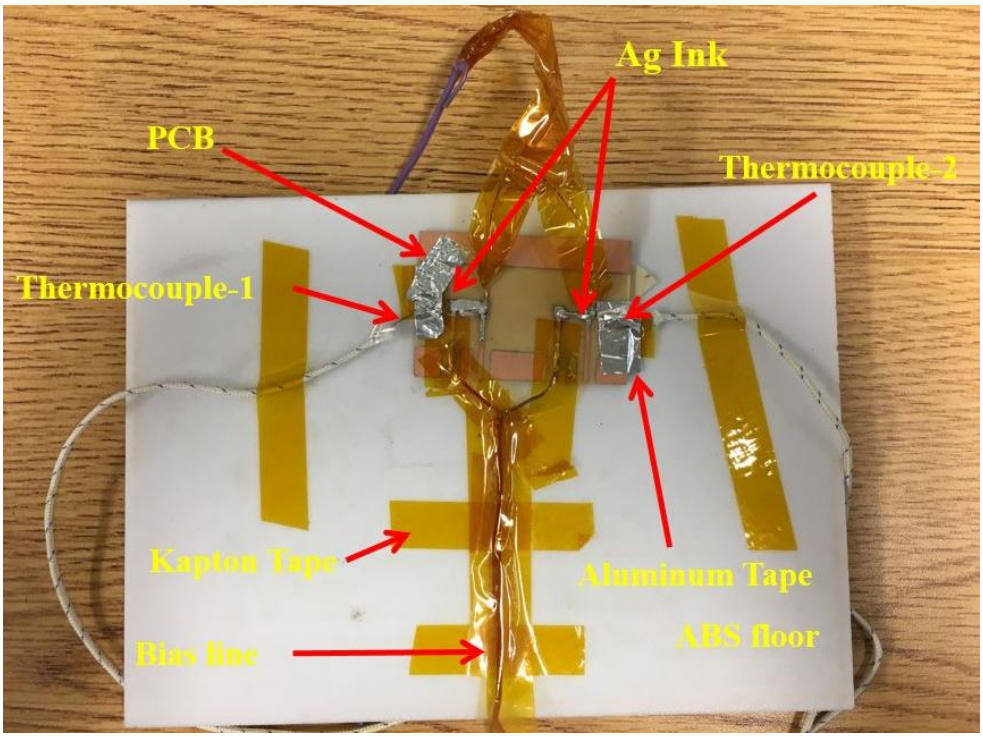

Figure 17: Experimental test sample preparation on 3D printed ABS floor

and high temperature testing, adhesion between thermocouple sensor and PCB may loose and disconnect the sensor part from the PCB Also, the aluminum tape provides the actual temperature of the test environment. Though the Kapton tape is an electrical insulator, it has high heat resistance up to 175˚C. Since the materials were dispensed on the PCB, it was essential to measure the ink temperature which was the PCB temperature. These two thermocouples were responsible for providing the temperature of the PCB.

3.5 Thermal test

To make the test procedures and experimental setups reliable, all the experiments were performed in two phases. First, the experimental procedures and tests data were verified in the Instron thermal chamber (HIGH WYCOMBE Model: 3119-609, Made in England). Secondly, a vacuum thermal chamber (Kurt J Lesker Company, Jefferson Hills, PA) was developed to test the conductive inks at low vacuum (10^{-2} Torr) and a -70℃ to 70℃ which was a representative of simulated space environment.

The Instron thermal chamber as shown in Figure 18, has the temperature control within the range of -150˚C to 350˚C but does not provide a sealed pressured environment. Low temperature

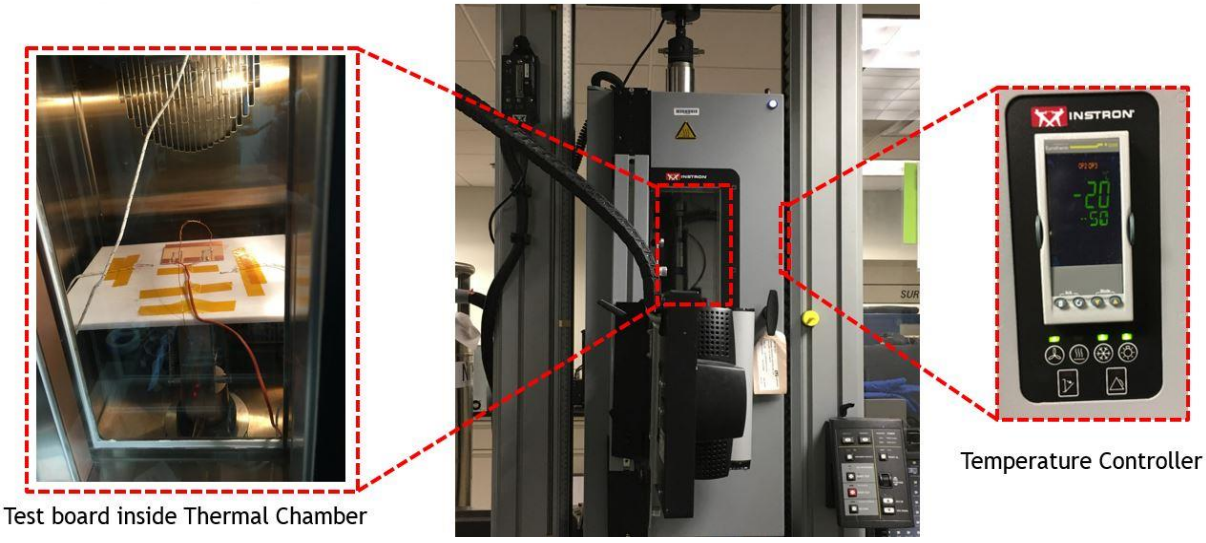

Figure 18: Low temperature testing facility of Instron thermal chamber

or cryogenic testing was done by circulating the liquid nitrogen (LN2) through shrouds which were placed inside the wall of the chamber. To know the temperature distribution inside the chamber one thermocouple was suspended from the top wall of the chamber to the free space, therefore the temperature above the ECI can be measured. The main challenge with the low temperature testing was moisture condensation over the specimen. Since the Instron thermal chamber did not have any system to expel the moist air, the pre-existing air inside the chamber condensed over the sample. Thus, the expected result was not obtained for cryogenic testing of ECI. Therefore, the necessity of a moisture removal system arose so that the cryogenics test result could be conclusive and comparable with the hot environment testing of the ECI. High temperature testing was done by operating built-in heater inside the back wall of the chamber. Since the ABS materials had the melting point of approximately 100˚C, the high temperature testing was done at 80˚C.

The test bed inside the thermal chamber and overall low temperature test facility of the Instron thermal chamber can be seen in *Figure 18*. The liquid nitrogen cylinder was at the rear side of the chamber which cannot be seen in the figure. The temperature controller on the chamber wall was used to regulate the temperature. For low temperature testing, there were the following three steps: i) connect the LN2 cylinder with the chamber ii) set the temperature such as -50˚C and iii) run the air circulator fan. For elevated temperature testing, the procedure was quite similar, although instead of the connecting LN2, the heater was needed to be turned on with pre-specified temperature and the fan was turned on as well. There was a consequent effect for operating the fan inside the chamber which will be discussed in the results and discussion section.

To accomplish the thermal cycle testing without the moist air and air circulation inside the chamber, the thermal vacuum system test facility was made. The most important and advantageous part of the thermal vacuum system was that the simulated space environment can be achieved. The

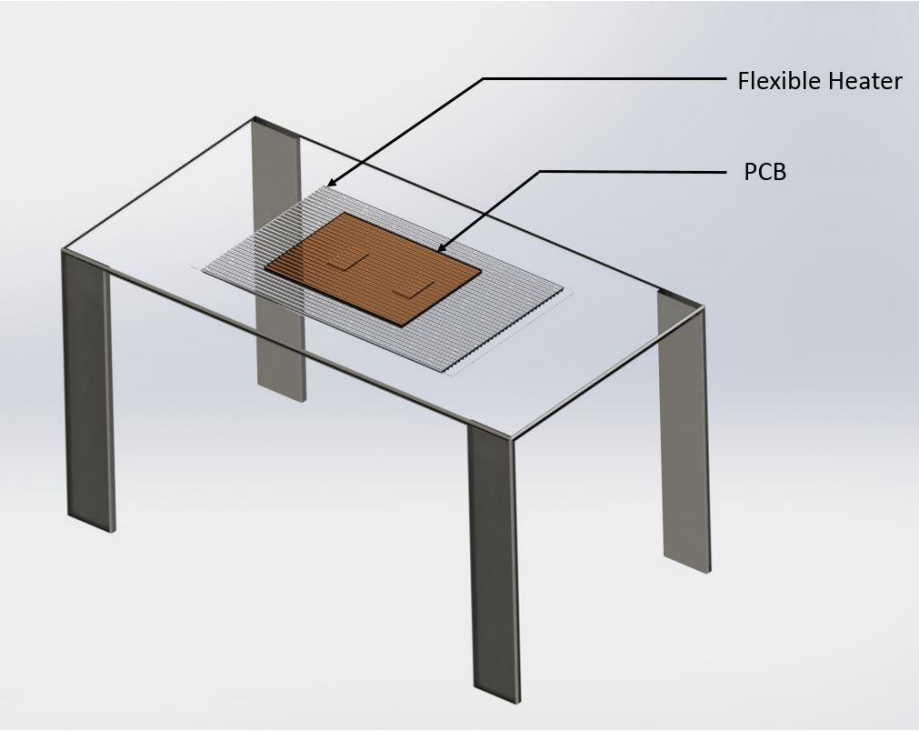

Figure 19: Heater table for elevated temperature test facility inside of the vacuum chamber

Hot environment was simulated using the heater. For vacuum application, a table heater was made using the Kapton® Polyimide Film-Insulated Flexible Heater (KH-510/2-P, OMEGA Engineering). The flexible heater was placed below the stainless-steel plate on the table. The table size was 30cm×18cm ×40cm which is shown in *Figure 19.* Since there was a direct connection between the heater and table, temperature rising time was very short (approximately 2 minutes). Therefore, a small distance (5mm) between the PCB and stainless-steel table allowed only the radiation heat transfer mode. The 5 mm distance was made by using the insulator tape. The high temperature test table was placed inside the vacuum chamber. The temperature of the heater was controlled by the AC voltage regulator, as the heater was AC powered. Rated power of the heater was 125W and it can create the high temperature up to 200˚C.

Low temperature test facility was made using the similar principle of the Instron chamber. Instead of the copper shroud to circulate the LN2, a copper block through hole was chosen for vacuum chamber. *Figure 20* represents the block diagram of low temperature test facility inside of a vacuum chamber. Using the feed through of the vacuum chamber, LN2 was passed through the copper block and dissipated the heat from the inside environment of the chamber. As a result, the temperature falls within a short period of time (approximately 5 minutes from room

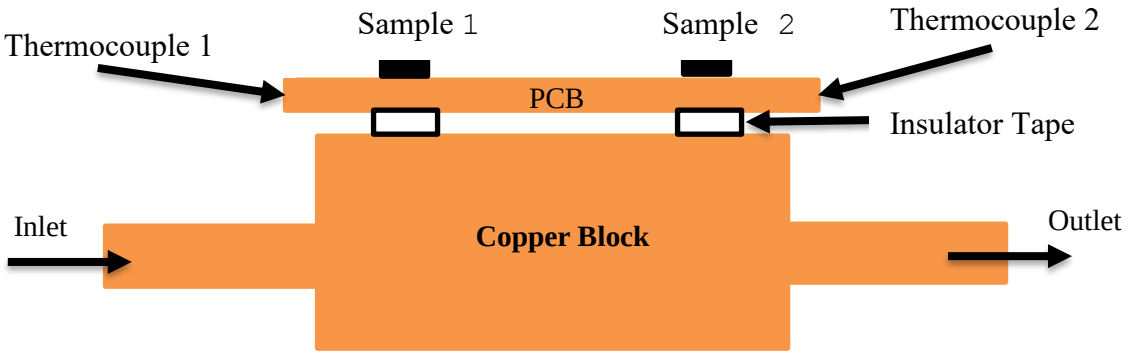

Figure 20: Low temperature test facility using the copper block.

temperature to -50ºC). In this experiment, the flow rate regulation of the LN2 was the temperature control mechanism.

Thermal vacuum system was operated by a mechanical pump (XDS 5, Edwards Vacuum LLC, San Jose, CA). Vacuum chamber has some feed through for the connection of thermocouple, LN2 circulation, and electrical connection as shown in *Figure 21*. The pressure gauge was monitored to collect pressure data. Only the test board was placed inside of the vacuum chamber

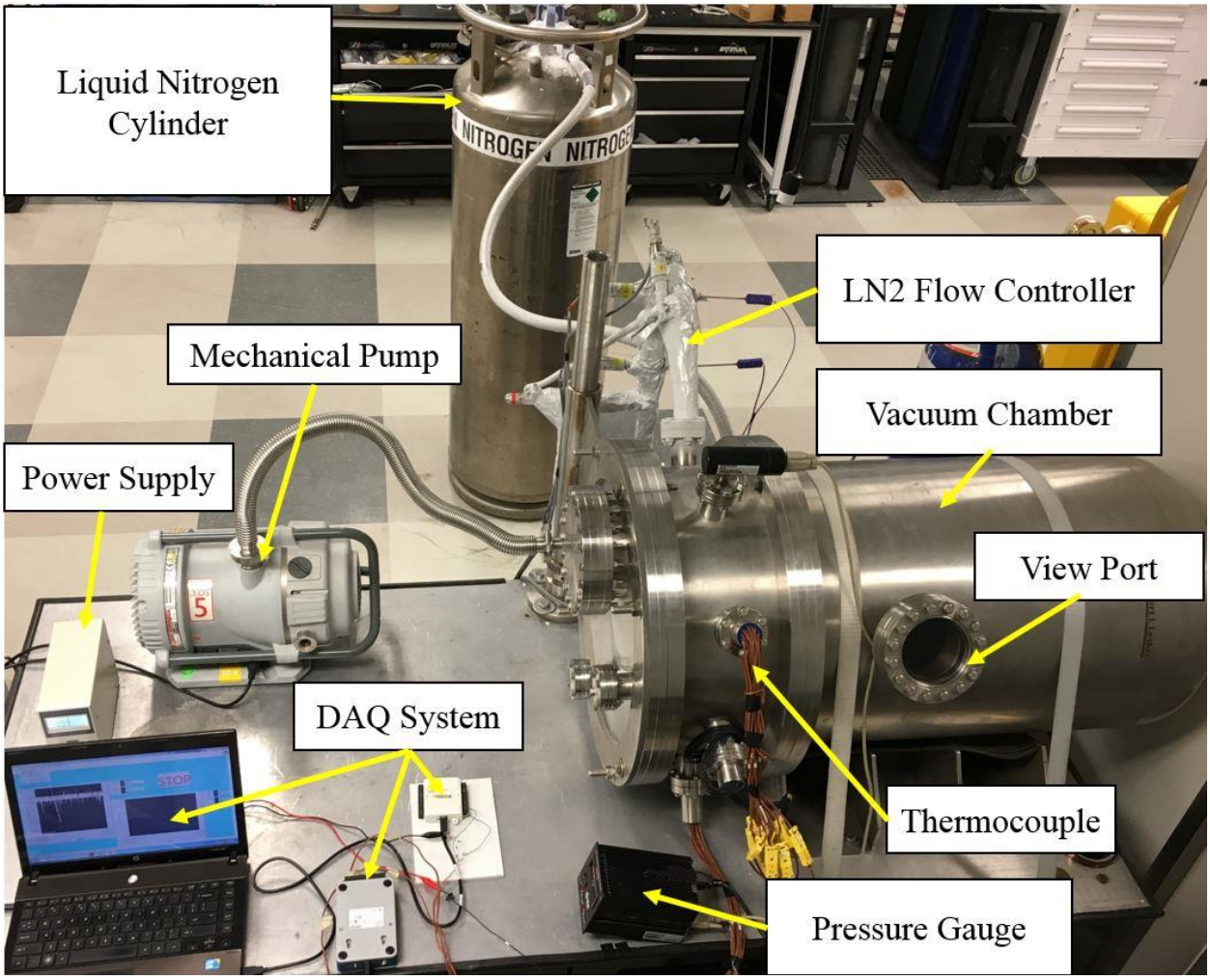

Figure 21: Experimental Setup of thermal vacuum system. Liquid Nitrogen flow controller used to change the flow rate and temperature for low temperature (-100˚C) testing. The heater table was placed inside the chamber which cannot be seen in figure was used for the elevated temperature (up to 125˚C) testing.

and rest of the electrical instrument and data collection instrument was placed outside of the chamber.

3.6 Electrical instrumentation and data Acquisition

Figure 22 shows the basic instrumentation schematic of the ECI testing in thermal environment. Resistance across each specimen trace was measured by creating the voltage divider with a known value of resistance and supply voltage. Since they were connected in parallel, voltage drop across the traces was same but the current flow was different. According to the parallel connection formula, output current was equal to the summation of the current flows through the individual resistance. In space, applicable solar array junction has 3.3V and 0.5A current flow. To simulate the similar environment and test setup, experiments were done using the supply voltage range 2-3.5V and the current range 0.01 A to 0.8A. The reason for choosing the low power supply through the trace was to avoid damage due to heat generation.

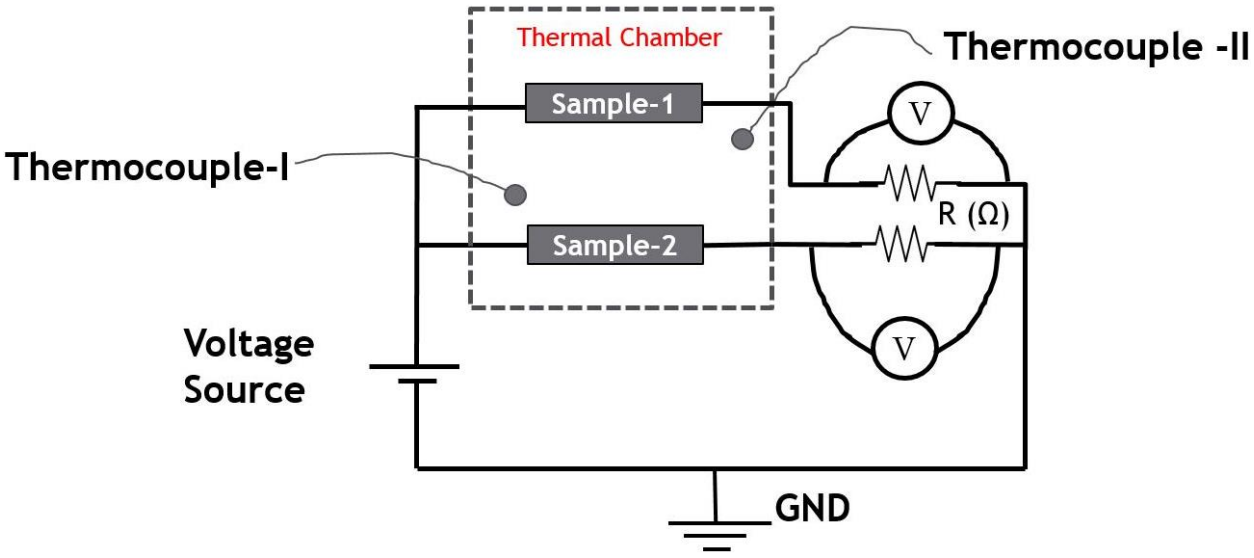

Figure 22: Illustration of experimental instrumentation for the ECI testing in thermal chamber.

The power supply (CSI3005SM, CircuitSpecialist.com) used for the experiment had capabilities of delivering 0 to 30V and 0 to 5A. By regulating the voltage and current, a standard supply was fixed for each experiment. The resistances used in the experiments were 10kΩ and 1kΩ. Since the value of resistance was known, the voltage drop across the trace and the current flow was measured according to the voltage divider rule.

A voltage DAQ (USB 6008, National Instrument) was used to measure the voltage drop across the ECI trace. Among two wires, first one was connected to the bias line of the trace and the second one was grounded with the power supply. A thermal DAQ (NI 9213, National Instrument) was used to collect the temperature data using the K-type thermocouples. Aforementioned placement of thermocouple was similar for all testing which includes two thermocouples on the PCB and one above the PCB to get the environment temperature.

LabVIEW software was used for the data acquisition system. Temperature and voltage DAQ was incorporated with the LabVIEW and then the control interface was made to control the experimental parameter. The data collection time interval was one second. LabVIEW program was made in such a way that it can collect and store the data of the time, temperatures, and voltages for every one-second interval. Additionally, the LabVIEW machine vision tool was used to measure the average gap between conductive particles after SEM image acquisition of ECI surface.

Chapter 4: Result and Discussion

Result and discussion chapter have following three major parts:

- ECI testing in thermal environment chamber (Instron)
- ECI testing in thermal vacuum chamber
- Physical appearance and microstructure analysis

Each part of the discussion consisting of the low temperature and elevated temperature testing result. Also, the result of spring test in the thermal environment discussed in this section. Finally, a conclusion was made based on the parameters of conductive path development and potential application of ECI in future AM in space.

4.1 Spring testing in low and high temperature conditions

Thermal testing results of stainless steel compression spring were confirmed that the spring can provide minimum required force 10.02 N in thermal environment, which was obtained from *Equation 9*. At low temperature (-50ºC), the spring constant was decreased to 1.05N/mm (at room temperature, the spring constant was 1.36N/mm) and at elevated temperature (80ºC) the spring constant was 1.29N/mm which were calculated from *Figure 23.* Elevated temperature testing led to the thermal expansion of the spring, which was responsible to the deformation of spring. Deformation in spring buckled under compressive load instead of the linear strain. Whereas at low temperature, the shrinkage of spring reduces the spring constant. At low temperature, spring material shrunk and reduced the free length by 2 mm (0.078inch). Therefore, the stiffness of the spring was affected at low temperature. Though the spring constant varied with temperature change, the exerting force was still under the limit i.e. it was providing more than 11N/mm force.

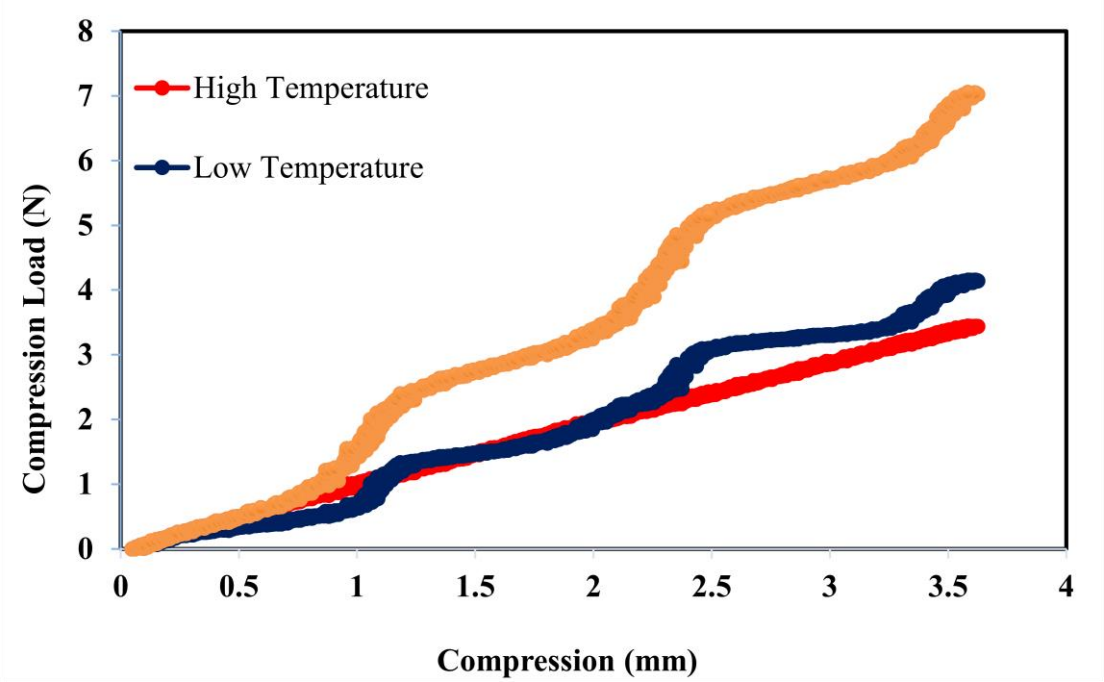

Figure 23: Variation of spring constant with respect to three different temperature (-50ºC, 22ºC, and 80ºC). Slope of each line represents the spring constant. For both high temperature and low temperature, spring constant was low as compared to the original

Therefore, this stainless-steel compression spring was selected for use within the injector to advance the plunger and dispense ink.

4.2 Thermal testing of ECI at atmospheric pressure

The author of this thesis would like to define the term curing in following way: curing of an ink is the development of conductive path on the ink surface, subsurface or bulk after being dispensed on a substrate. This curing is not concerned about the fully cured trace rather the time required to achieve maximum current flow data. Maximum current flow data for each test refers to the current carrying capacity of conductive ink traces that was supplied from a power supply. For each test, there was some loss in current flow (40% of the total supplied current) because of

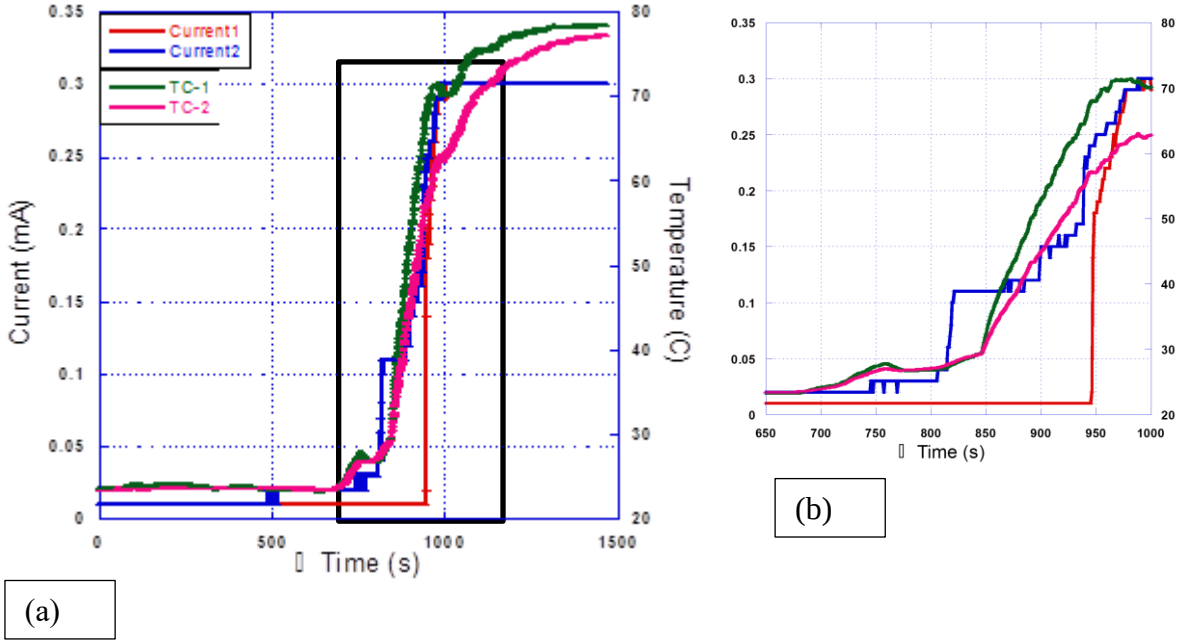

Figure 24: (a) Conductive behavior of E1660 at elevated temperature (80˚C) under atmospheric pressure (b) Zoomed out of selected area between 650s to 1000s.

heat generation and electrical cable connections. Therefore, a maximum current flow 0.6mA was found against 0.9mA supplied current.

Initiation of current flow time of both ECIs (DuPont CB 102 and Ercon E1660) was measured in a thermal chamber at atmospheric pressure. In the thermal chamber, two different types of testing were performed. At first, the high temperature (70°C) testing of Ercon E1660 was done at the Instron thermal chamber by running the heater and air circulation fan. Current 1 and Current 2 represents the flow of current through the specimen 1 and specimen 2 respectively in *Figure 24*. TC-1 and TC-2 represent the temperature of each specimen which was collected using the thermocouple sensor next to each specimen on PCB.

Both specimens on the PCB were the same materials at the same time (each test). The main reason to choose the same material was to mitigate the risk of variation in testing data. The result

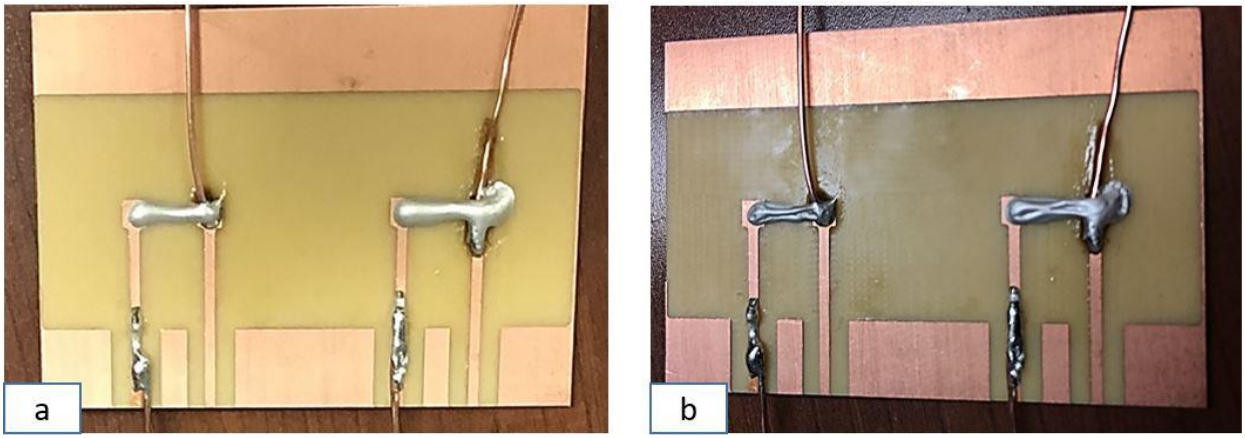

Figure 25: (a) Liquid or semisolid ink before elevated temperature testing and (b) shrunk ink after high temperature (80˚C) testing. Continuity results obtained due to the surface and sub-surface dryness of the ink.

of two specimens with similar material provided a better understanding of time and temperature dependent conductivity phenomena.

For specimen 2, initiation of conductivity was found at 28ºC and maximum current flow (0.3mA) obtained at 72ºC. The total time to provide the maximum current flow (0.3mA) for sample 2 was approximately 250s. In case of specimen 1, the initiation of current flow was found at 55ºC. The time required to reach maximum current flow (0.3mA) through specimen 1 was short (approximately 50s) as compared to the specimen 2. Zoomed out area of *Figure 24 (b)* represents the temperature increasing rate which was 0.28ºC/s. For specimen 1, exposure to high temperature (70°C) environment reduced the evaporation time and shorten the time to initiate the current flow. The reason for the variation in the initiation of conductivity time of both specimen was the trace thickness.

Initiation of conductivity through the ink trace depends on the surface and subsurface desorption rate. As the thermal desorption from metal solution is a surface phenomenon [74], solvent desorbed first from the exposed surface. As a result of desorption or evaporation of the

solvent, the surface layer of the ink conducts electricity by creating a conductive path. Also, the evaporation of the solvent was responsible for shrinking the ink trace by creating the space to accumulate the silver particles together. *Figure 25* represents the ink physical appearance before and after the curing. Two specimens had different trace width and thickness. Specimen 1 had thick trace and larger surface area as compared to specimen 2. The relatively larger surface area was taking a long time to initiate the curing but once the subsurface cured at 55ºC, it delivered the full amount of current (0.3mA). On the other hand, specimen 2 smaller surface area which accelerated the curing process. Since the resistance is inversely proportional to the surface area, the larger surface area has less resistance to flow the current. Although specimen 2 was started to conduct electricity early, due to the larger subsurface surface and cured area specimen 1 conducted a full amount of current within a short period of time. It is worth to mention that the bulk of the ink was not completely solid and this was confirmed by physical contact with a metallic probe.

CB 102 was tested under the similar environment to determine the curing properties as shown in Figure 26. Sample 1 was conducted a small amount of current (0.03mA) from the time of dispensing the ink on PCB. At room temperature (22ºC), current flow was increasing with respect to time (up to 240s). When the heater was heating the specimens at the rate of 0.12ºC/s, specimen 1 started to cure or provide continuity (current flow through specimen) by evaporating the solvent in a linear relation i.e. conducting current was proportional to the increment of heat. For specimen 2, conductivity was initiated at 240s (4 minutes) from the beginning of dispensing of conductive paste on PCB. The subsurface of specimen 2 cured within a short period of time (96s according to the raw data) due to the small thickness of the trace. The curing curve was similar to the E1660 but the remarkable point was the initiation of conductivity time after the ink being dispensed on the substrate. Though the current flow through the ink trace was initiated at 21˚C,

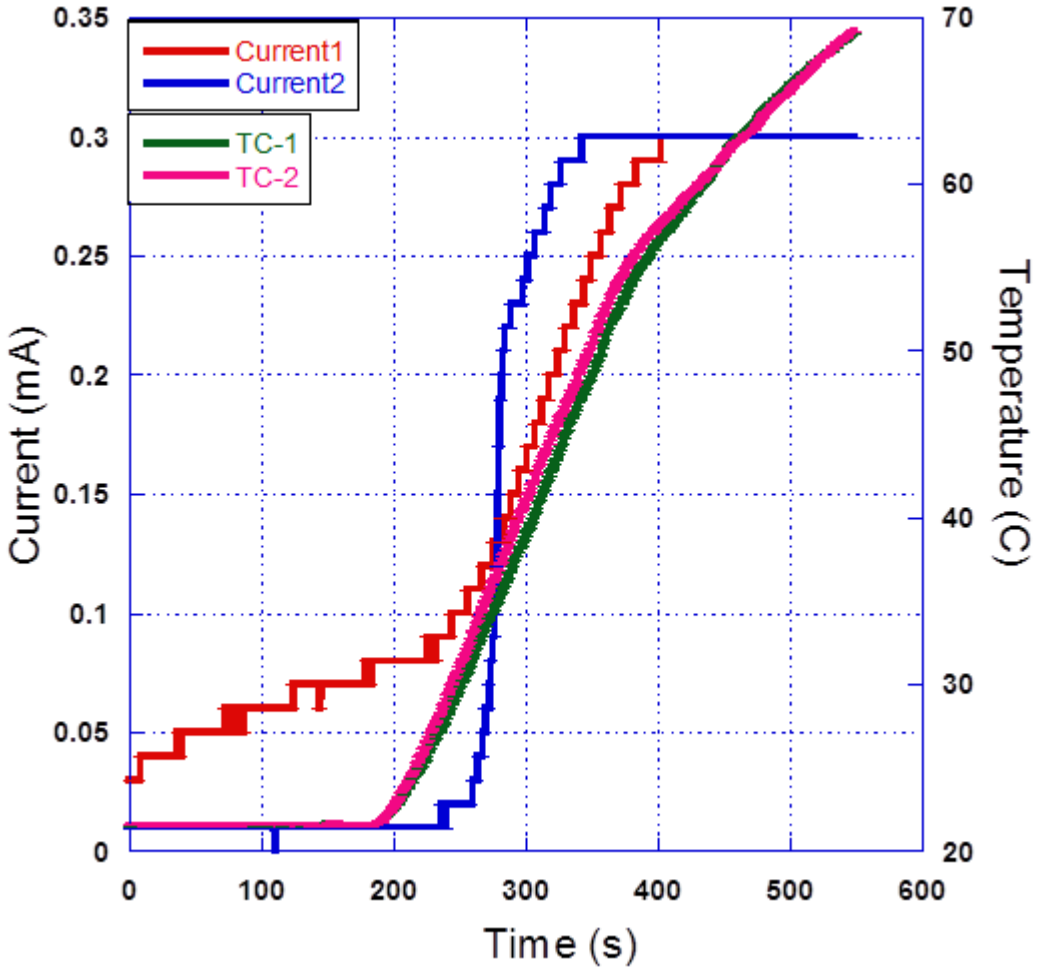

Figure 26: Relation between the temperature and current flow of CB102 when tested at elevated temperature (70˚C) and atmosphere pressure.

the maximum current flow (0.3mA) was found after 62˚C. Since the CB102 possesses the high viscosity and the solution started to evaporate to the environment at room temperature, it took a short time to cure and provide the continuity as compared to the E1660.

The early initiation of curing determines the ability to conduct electricity with shortest possible time. Though the total supplied current flow was 0.9mA from the power supply, each specimen carried only 0.3mA current. As the test setup of the circuit was divided the current flow using the parallel connection of resistance, the aggregate current flow was 0.6mA. More than 40%

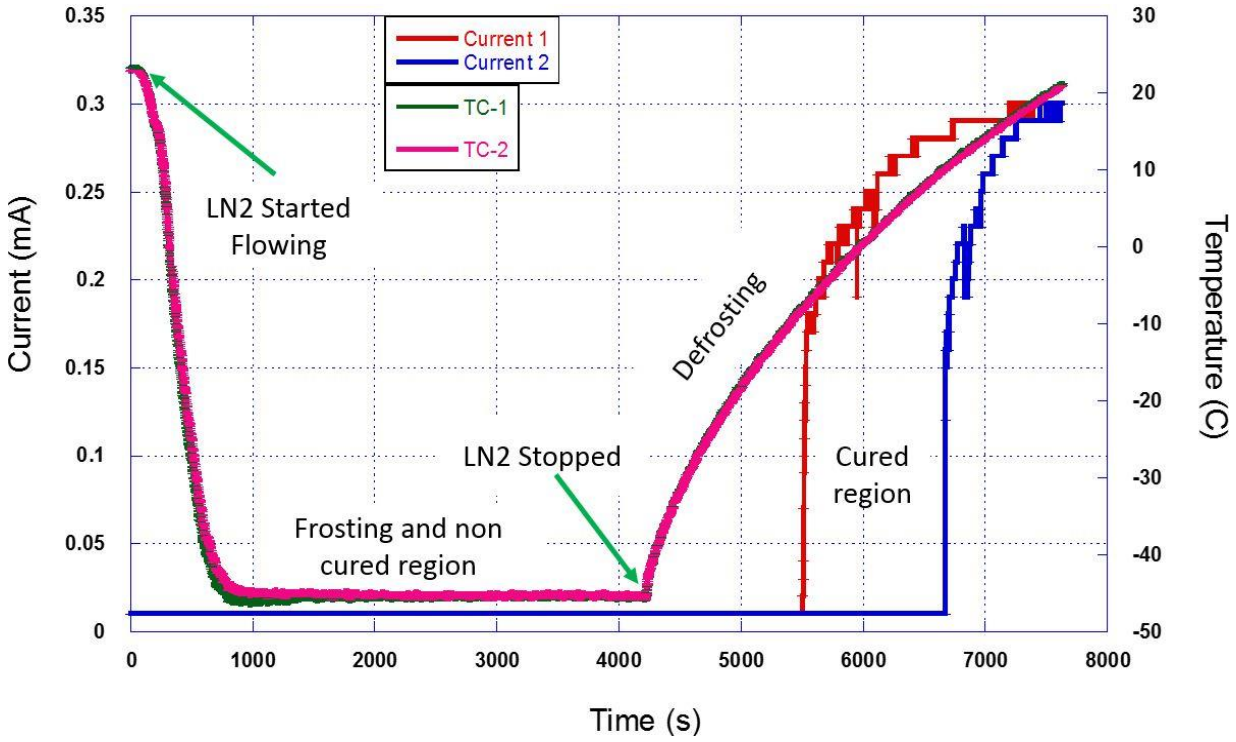

Figure 27: Graphical representation of challenges in low temperature (-50˚C) testing of E1660 ink in environment chamber. Initiation of conductivity time was affected due to the frosting and defrosting. over the ink.

loss in current flow occurred due to the heat generation in trace and wiring between the test bed inside of the chamber and power supply which was placed outside of the chamber.

Low temperature testing of the ECI had some challenges in the Instron environment chamber. There was no such way to remove the moist air from the chamber. During the low temperature testing, there were two different regions on the curing curve, frosting and defrosting in *Figure 27*. When liquid nitrogen (LN2) started to flow, the temperature decreased steadily to -48˚C. There was no current flow through the ink for more than 1 hour. When the fan and LN2 flow stopped, the temperature was increased. As a result of that, defrosting occurred on the ink and electricity flow was initiated.

Additionally, the defrosting on the ink surface hydrated the ink and reduced the viscosity. As a result, the ink had more liquidity. This was confirmed by the physical appearance; the ink swelled on the PCB and the top surface was completely wetted. Therefore, the low temperature testing within the Instron environment chamber was not sufficient to provide the curing characteristics at cryogenic condition. Overall thermal testing at an atmospheric pressure determined the validity of the test procedure and suggested to continue the testing under vacuum condition, so then the testing results reflect the conductive characteristics at space environment.

4.3 Thermal vacuum testing of ECI

Thermal vacuum testing of ECI consisted of testing at elevated temperature and low temperature. Most of the space applicable materials experience the high temperature due to direct sunlight, and low temperature is experienced in the absence of light (dark condition). Therefore, materials and dispensing mechanism for space application need to be tested under high and low temperatures. The advantage of conductive ink dispensing at high temperature environment is the reduced time to achieving the maximum current flow. Due to the accelerated polymerization and cross-linking rate at high temperature, the process of creating conductive trace takes short time compared to the low temperature environment. The room temperature testing was conducted to corroborate curing information provided by the ink manufacturer. In this section, thermal tests were described by following sequences: high temperature, low temperature, and room temperature. The test procedure for vacuum thermal system was similar to the Instron environment chamber. Only the test board, heater (high temperature test facility) and copper block (Cryogenic test facility) were placed inside the chamber. The remainder of the electrical circuit was placed outside the vacuum chamber.

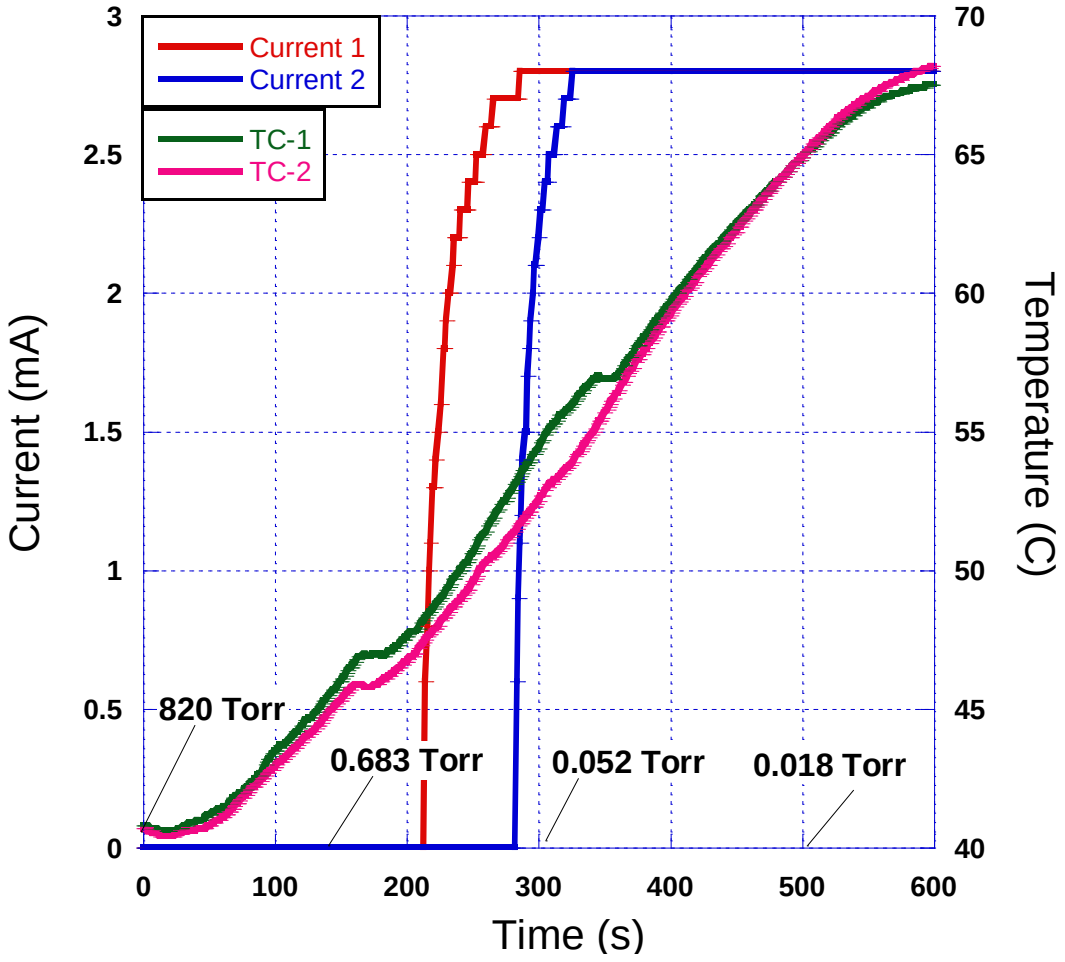

Figure 28: Conductive behavior of E1660 in thermal vacuum system. Elevated temperature (70°C) and vacuum pressure (10^{-2} Torr) accelerated the initiation of conductivity process which indicates that the ink trace will conduct current after being dispensed in space environment as well.

In the vacuum environment, high temperature testing of E1660 resulted in quick evaporation of the solvent within the ink. Initially, the system had a chamber pressure of 820 Torr (1atm=760 Torr). Also, the system was preheated at 41ºC before running the test. and temperature of 41˚C. Temperature was increased steadily and pressure decreased due to expelling the gas from the chamber. For each experiment in thermal vacuum system, reduction of the pressure level inside the vacuum chamber was rapid at first (decreasing from 820 to 0.25 Torr within approximately the

first 200 seconds), and slow towards the end where a pressure of 0.018 Torr was constant for 10 minutes. The initiation of conductivity started at 45˚C and 9.31×10^{-1} Torr. For both specimens, the total time required to create a conductive path that allowed to flow electricity was less than 60s as shown in *Figure 28*. Though the full conductive path development temperature was above 50˚C, the testing continued to investigate the topographical condition of the ink, which is discussed later in this section.

At low pressure, trapped molecules on the surface and subsurface expanded, as a result outgassing occurs. Additionally, the elevated temperature during testing excited the process of gaseous molecules leaving the subsurface, and the same can be said about low vapor pressure molecules from the top surface. Only the particles that have the higher vapor pressure linger on the substrate. Depending on the conductive particle size and structure, accumulation occurs among them to fill out the void space and create a conductive path. This accumulation leads the current flow across the bulk of the ink materials.

Effect of particle size in the conductive path development process can be demonstrated by the high temperature testing result of CB102. Higher packing density between the nanoparticles as compared to the flake-based particles enhances the process of conductive path development, i.e. reduces the time to develop a conductive path on the surface or subsurface. The Higher packing density of the nanoparticles after the evaporation of the non-polar solvent is responsible for conducting electricity. Though the CB102 took a long time to provide current flow data (500 seconds as opposed to 320 seconds for E1660), the initiation of current flow time from the beginning of dispensing (200 seconds) indicates the possibility of premature solidification (curing) of the paste.

In Figure 29, a conductive path on both specimens was developed at 44ºC and pressure level 0.37 Torr. Both specimen traces had a similar thickness, hence the continuity curve was very close to each other. After 480s (8 minutes), both of the traces were conductive i.e. they carried 2.73mA current. As the pressure decreased and temperature increased continuously for first 10 minutes, the solvent vapor pressure of the ink reduced. Lowered vapor pressure led the conductive particles to increase the packing density (reduced the distance between conductive particles) on the surface and surface, thus continuity was found within 0.37 Torr to 0.021 Torr as marked in

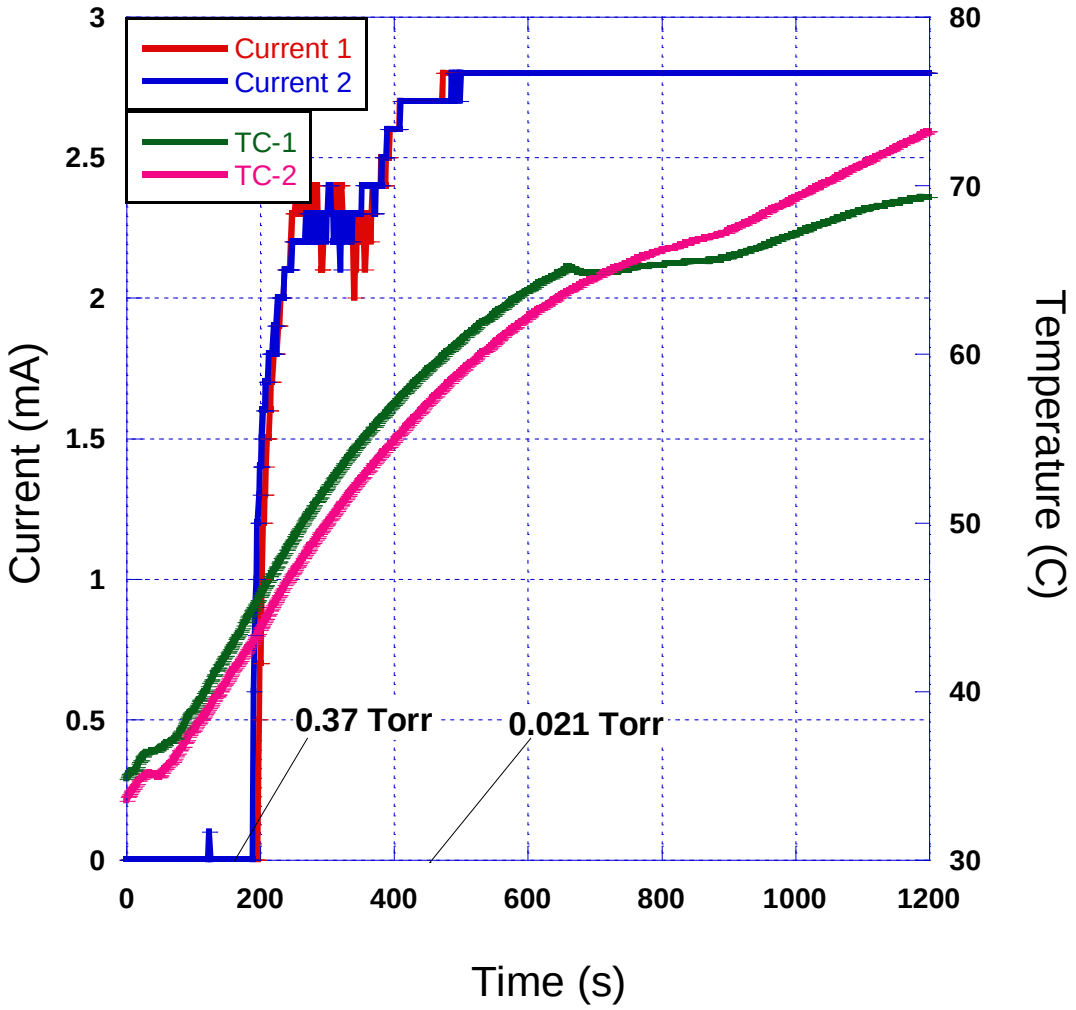

Figure 29: Early conductivity of CB102 at elevated temperature indicates the quick evaporation of the solvent. Total time to obtain maximum current flow through the ink traces was 318s.

Figure 29. Hence the point of interest in pressure was that pressure which is responsible for initiating the current flow through the ink.

LN2 has the boiling temperature -196˚C. Therefore, it continued to cool down the temperature of the copper block during the low temperature testing. After 30 minutes, the flow of LN2 was stopped because the maximum current flow was achieved at that point. For the reliability

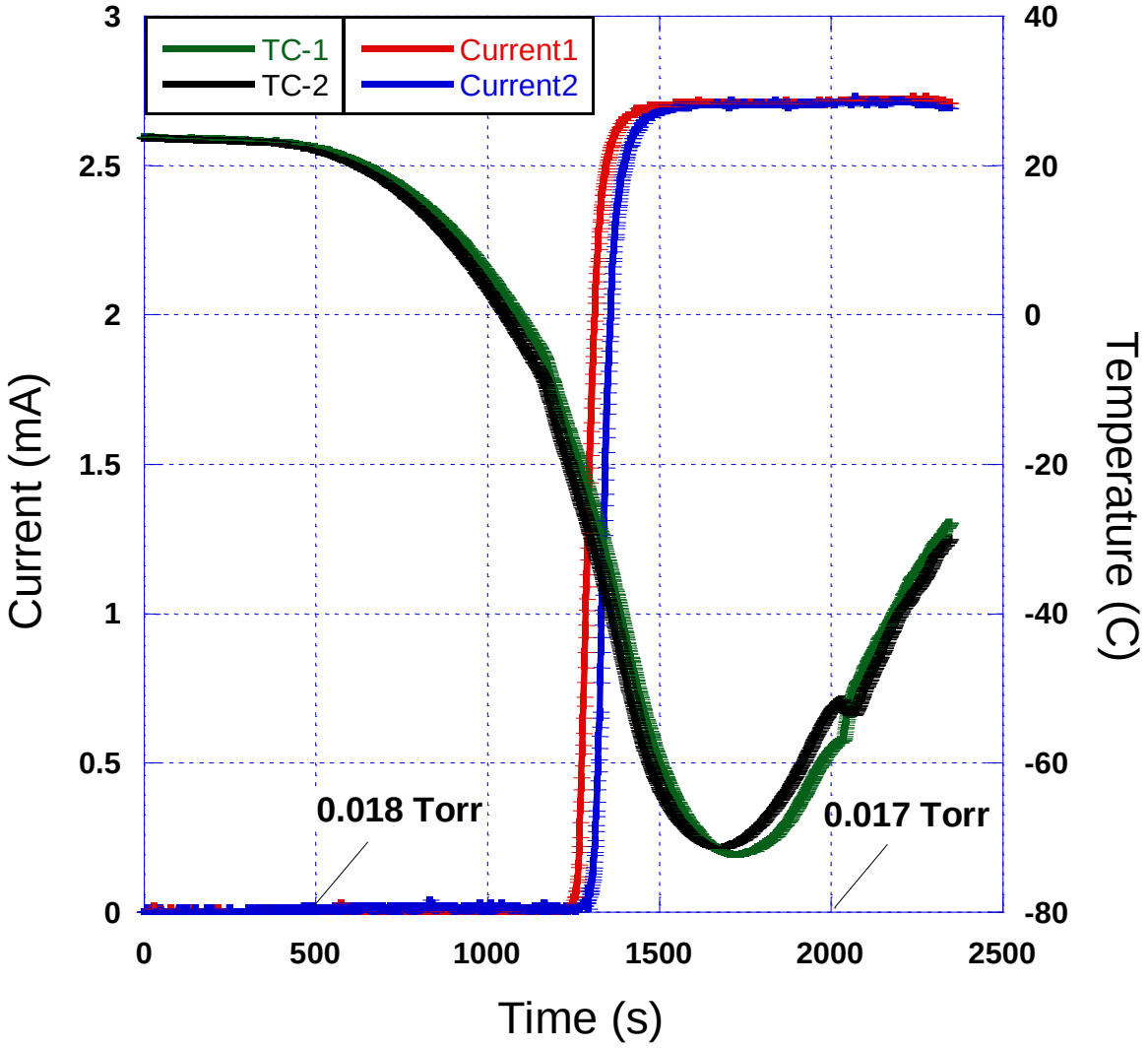

Figure 30: Delay of the initiation of current flow of E1600 was found at cryogenic temperature in vacuum chamber. Conductivity was found within the temperature range of -28˚C to -38˚C. Maximum current flow (2.7mA) was achieved in both specimens at 1500s.

of test data, long period testing (more than120 minutes) was performed and the temperature was also less than -100˚C. Long period testing was conducted because it was not confirmed whether the current flow was from surface or sub surface curing or moisture particles on the ink surface. To confirm the reason of current flow, long period testing was performed hence all the moistures were removed from the vacuum chamber and maximum current flow was obtained because of evaporation of binder polymer from conductive particles. In the low temperature cases (when using CB102 or E1660), the conductivity characteristics were similar to each other. The benefit of the cryogenic tests was that there were no frosting or defrosting issues when using the vacuum chamber. Continuous removal of air and gas molecule from the chamber helped to prevent the frosting inside the chamber. Thus, the low temperature testing was not affected by any external agent as was the case with the Instron thermal chamber. Also, the vacuum level was almost constant over the entire test period.

As seen in *Figure 30*, the lowest vacuum was achieved at 500s and it was constant until 2500s. The test was started at room temperature and atmospheric pressure. As time increased, pressure and temperature were decreasing. At -20˚C, initial continuity was obtained and full continuity was achieved within the next 200s where the temperature was -72˚C. After achieving the full continuity, LN2 flow was stopped but the temperature continued to decrease to values below -30˚C. Therefore, the low temperature and vacuum testing of E1660 demonstrates the capability to develop a conductive path by evaporating the binder from the ink. The comparison between two promising inks was possible after the low temperature testing of CB102 at thermal vacuum environment. CB102 was tested (as shown in *Figure 31*) in such a thermal cycle that had the initial temperature of 18˚C and the lower temperature of -58˚C. Though the experiment was started below room temperature, the low temperature range was limited to -18˚C to -58˚C. After

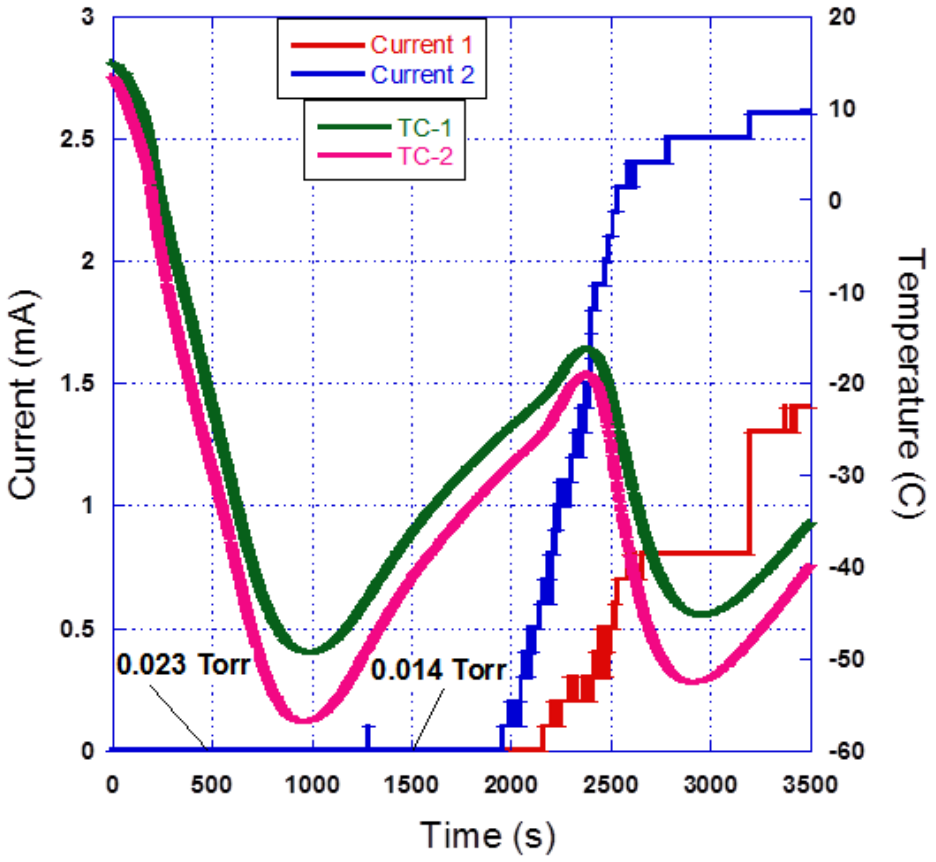

Figure 31: CB102 tested at low temperature cycle; current flow was affected due to the low temperature.

conducting several experiments in similar temperature profile, it was observed that the initiation of polymer binder solidification (development of conductive path) was delayed in CB102. Pressure level inside the chamber was maintained similar to the E1660 testing; lowest pressure level was 10^{-2} Torr after 8 minutes and remained constant until the end of the experiment.

From *Figure 31*, CB102 was able to develop a conductive path after a long period of testing (2000s) as compared to the E1660 (1200s). Specimen-1 had higher trace thickness, hence it failed to provide a maximum current flow (2.7mA) over the entire period of testing. Higher the trace thickness had a larger amount of polymer binder presented on the ink. According to Clausius-Clapeyron equation *(Equation 9)*, the relation between the temperature of the liquid ink and its

vapor pressure is inversely proportional to each other. As the vacuum system temperature went down, the vapor pressure of liquid increased. Therefore, polymer binder in CB102 was not completely solidified or evaporated at low temperature and pressure. Partial solidification or evaporation of binder allowed to flow the current of 1.4mA, whereas the specimen 2 had small trace thickness allowed the current flow of 2.6mA. The solvent had a higher vapor pressure at a low temperature, as is generally seen with other solvents at a low temperature which in this case prevented the solvent from volatilizing and delayed the continuity result.

For space application, it is important to develop a conductive path within the shortest possible time after dispensing the ink. If a material is not completely cured but providing the continuity and fulfilling the low outgassing requirements then still it can be considered as dispensing material. Curing of conductive ink may take long or short time depending on the dark and sunlight condition. At sunlight condition, ink will experience elevated temperature (40℃ to 150℃ depending on the orbit and altitude) that promotes ink curing process. In absence of sunlight, ink will experience low temperature (5℃ to -70℃ between LEO and GTO) that slow down the curing process. Therefore, at low temperature (below 4℃) instead of curing, a conductive path is important to

Table 7: Summary of the thermal vacuum testing of ECIs.

Ink	Temperature	Carried current	Time at which current has present (s)	Temperature of continuity (˚C)
E1660	Low	Yes	1200	-28 to -30
	High	Yes	225	45 to 48
CB102	Low	Yes	2000	-20 to -30
	High	Yes	200	45 to 50

connect two terminals of the damaged solar panel to complete the circuit and charge the battery or power house. All experiments were conducted to determine the time required to solidify the binder or evaporation of binder to develop a conductive path on the surface and subsurface of the ink trace.

Table 7 represents the summary of thermal vacuum testing of ECIs. At low temperature, CB102 had delayed in conducting electricity as compared to E1660. Though both inks conducted electricity at low temperature and elevated temperature, E1660 was more promising for DW in space. CB102 needs a very sophisticated dispensing system and conditioned space, else it will be cured before dispensing. Especially at elevated temperatures handling CB102 is associated with high risks in terms of premature curing than E1660 is. Additionally, a long shelf life at room temperature is helpful for the mobility and design of a low-cost dispensing system. As the E1660

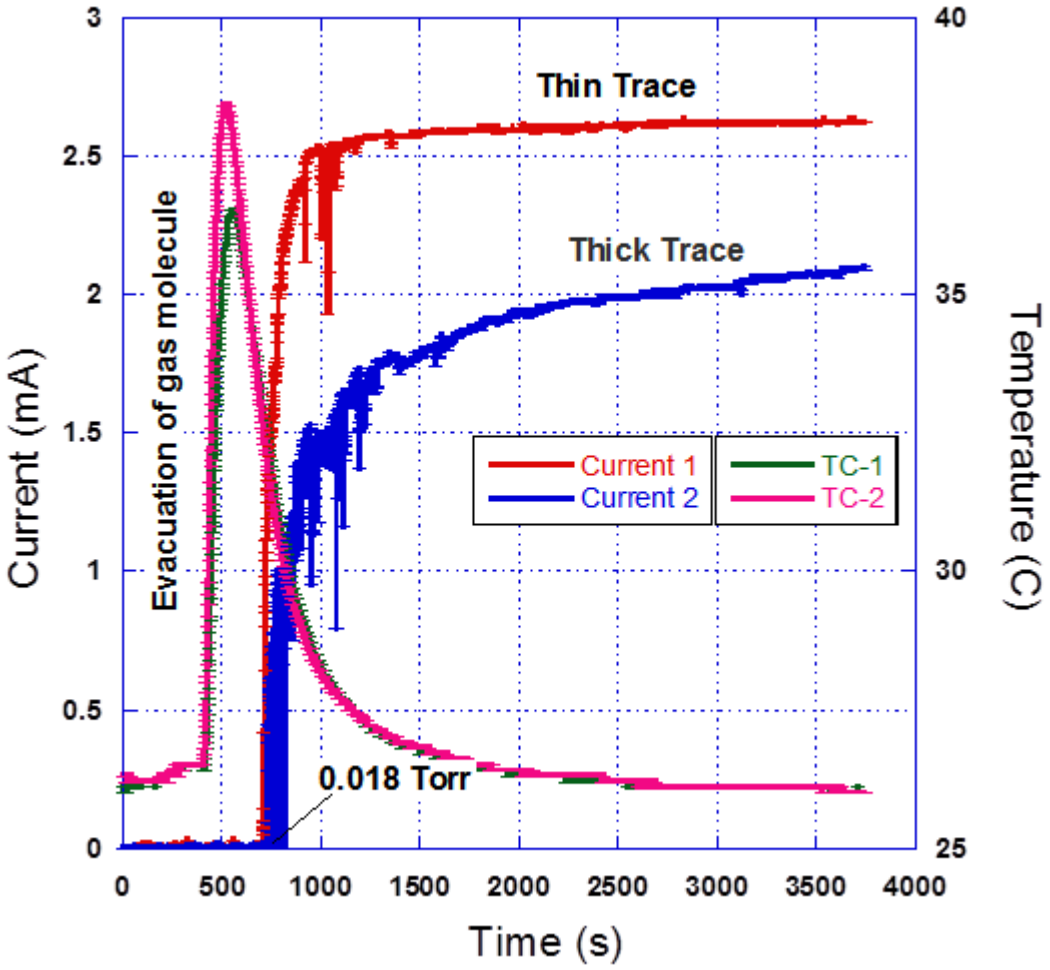

Figure 32: Vacuum testing of E1660 at room temperature. Temperature inside the vacuum chamber was increased by 10˚C for each experiment after starting the rough pump. Gas molecules moves with Brownian Zigzag movement that increased the kinetic energy; ultimately increased the temperature inside of vacuum chamber. After complete evacuation of gas molecules, pressure was 10^{-2} Torr and temperature came to the room temperature at 2000s.

showed the ability to provide continuity in a wide range of temperatures and had no premature continuity at room temperature, one further test in the vacuum chamber was conducted.

Room temperature testing result (*Figure 32*) in vacuum environment demonstrated the continuity test result in low pressure. Both specimens started to conduct electricity at 758s. Current

flow curve of both specimens had a similar pattern but thin trace carried 2.6mA and thick trace carried 2.1mA current after developing a conductive path. The reason for variation in continuity results already discussed in the previous test. The subsurface of ink trace was not completely cured; it was confirmed by the physical appearance. The resistance offered by the specimen 2 was greater than the sample 1. Differences of the resistance between two inks were found due to the thick (specimen 1) and thin trace (specimen 2) of the ink. So, the thickness of the trace was a variable for ECIs curing process. Higher the thickness of trace, more it will offer the resistance to conduct electricity. The room temperature testing provides the undesired properties of CB102 which is premature curing. Premature curing reduces the shelf life and decreases the reliability to shipping from one place to another place. As a result, only E1660 was chosen to dispense in space environment using a 1U small CubeSat.

4.4 Physical appearance and microstructure after thermal vacuum testing

In a vacuum environment, the trapped molecules from the surface and subsurface created bubble formation, which ultimately was responsible for outgassing of materials. Physical appearance of both samples after being taken out of the vacuum chamber contained bubble formation (*Figure 33*). The surface of the CB102 was damaged due to the bubble formation and destruction. Interestingly, the surface of the E1660 was not damaged (i.e., no perforations), rather the ink surface tried to stick to the substrate. The solvent of E1660 wetted the substrate and made a bond to adhere the conductive particles with substrate. Since the evaporation of the solvent occurred in thermal vacuum system, trace shrinkage was evident for each testing of E1660. For CB102 there was some shrinkage and smaller than the E1660. Adhesion of liquid materials to the PCB substrate in low pressure system is a promising characteristic of an ink to be employed as the dispensing materials to create a conductive path in an electrical circuit or solar panel in space

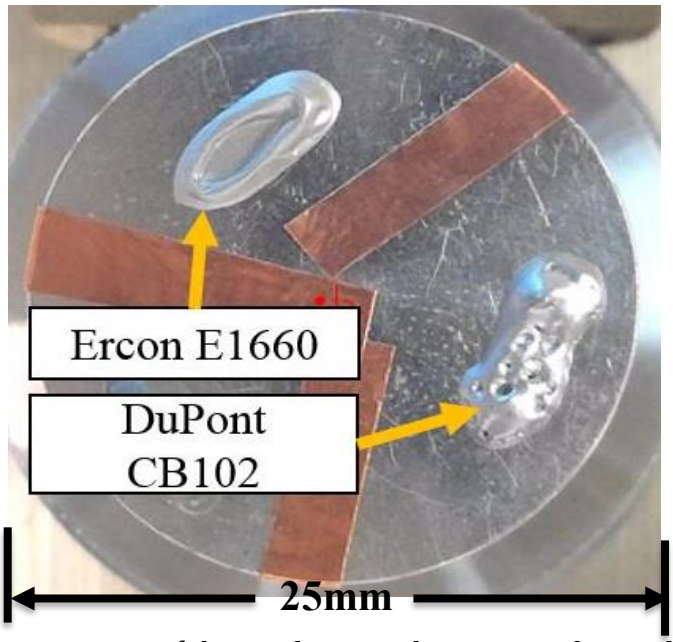

Figure 33: Physical appearance of the conductive ink traces. Both samples were dispensed on an aluminum pot. The pot was placed inside the vacuum chamber for 1 hour to visualize the change in physical structure.

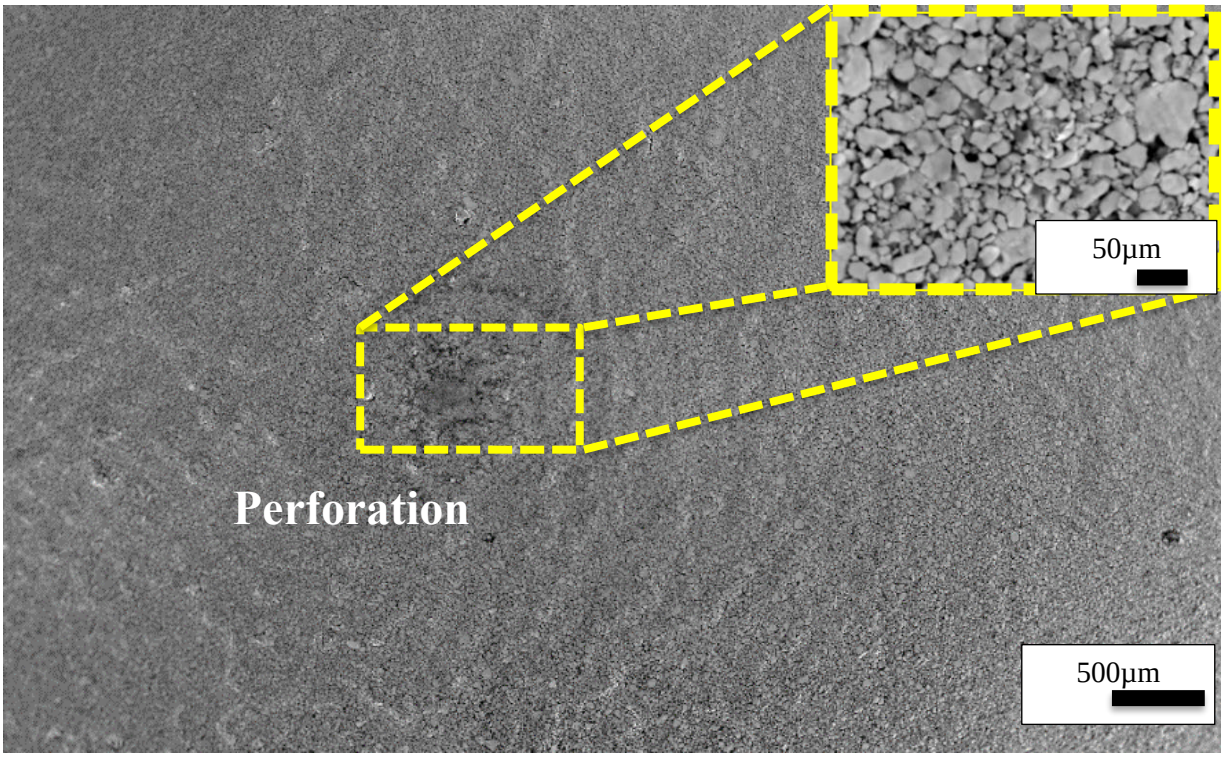

Figure 34: SEM image of CB102 was taken after curing in thermal vacuum system.

Evaporation of solvent from the ink created the pore which can be seen in 50µm zoomed in environment. Cured and adhered conductive material will serve the purpose to join two terminals and conduct electricity through a closed circuit.

For better understanding and studying the microstructure of the ECIs trace surface after thermal vacuum testing, cured specimens (E1660 and CB102) were taken under Scanning Electron Microscope (SEM). There were two distinct regions on the ink surface referencing to *Figure 34* the dark or black sections are gap between silver particles and white sheds are the silver particles. The gap between silver particles in the CB102 ink on the surface layer was found when closely looking at SEM image. Bubble destroyed section *Figure 35 (a)* was captured in 50µm

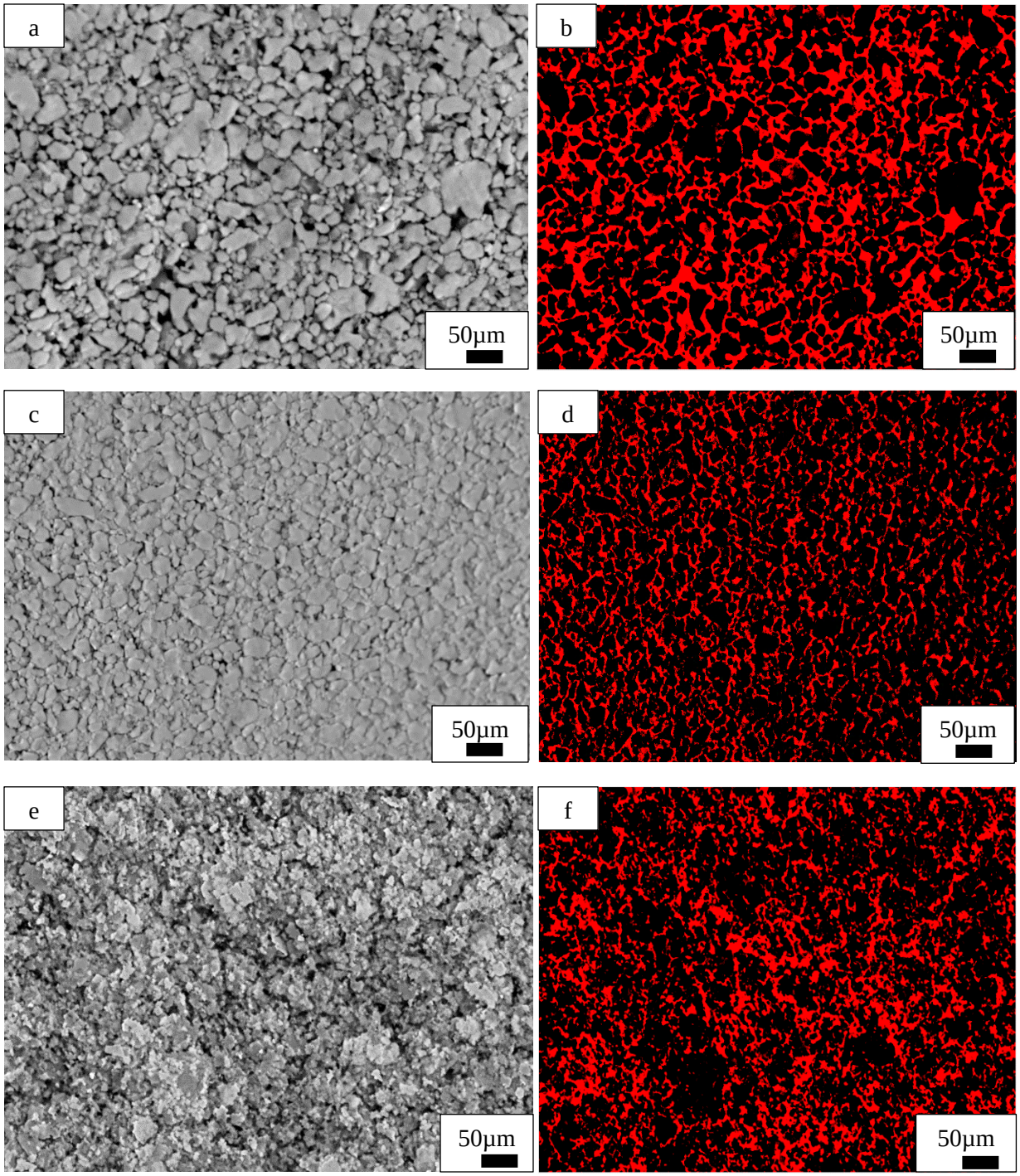

Figure 35: (a) Perforated section on CB102 ink surface (b) Measurement of gap area on perforated section of CB102 surface (c) Plane surface of CB102 (d) Measurement of gap area in plane surface of CB102 surface (e) Surface microstructure of E1660 and (f) Measurement of gap area on E1660 surface.

amplification SEM image to investigate the gap between conductive particles. Quantification of

the gap between conductive particles was done using LabVIEW machine vision tool. *Figure 35* represents the images of CB102 (a, b, c, and d) and E1660 (e and f) that acquired before and after image processing in machine vision tool. Red area detected as the gap between silver particles and the black area was silver particles. The point of interest was the bubble destroyed section of the ink layer. Bubble formation in ink trace reduces the cross-section area that leads to higher current and potential over-current fusing. For CB102, two different section of surface microstructure was investigated by incorporating the SEM image in machine vision tool. In the perforated section of CB102 ink surface as shown in *Figure 35 (b)*, the average area of the gap between silver particles was 245µm^2, whereas rest of the plane surface had average area 107µm^2. For perforated section, the particles area was 76% and gaps area was 24%. *Figure 35 (c)* and *(d)*, are representing the images of plane surface area of CB102 ink. It was measured that 92% of the surface area was the conductive particles. *Figure 35* (e) and (f) are representing the image of E1660 before and after the measurement of gaps area between silver particles. The average area of the gaps on E1660 was 110um^2. Area of the conductive particles on the surface was 94% and gaps area was 6%. *Table 8* represents the quantitative comparison between CB 102 and E1660. In CB102, bubble destroyed section had the higher gaps as compared to the plane section. On the other hand, E1660 had fewer gaps area. For conductivity and surface finish after curing the ink trace, less or no bubble formation and destruction is desirable.

Also, the affinity to adhere with the substrate material is an important part, because at vacuum environment it is necessary to adhere with substrate with sufficiently strong forces; therefore, the solidified material will not evaporate anymore. When working with conductive inks, another important characteristic is the current-carrying capacity or ampacity, which is the current that can pass through the trace after making a complete conductive path without overheating or

Table 8: Comparison between the area of gaps and the area of silver particles in CB102 and E1660

ECI name	Section	Conductive particles area (μm^2)	Area with gaps and conductive particles (μm^2)	Percentage of conductive particles area (%)	Allowable percentage of error for analysis
CB102	Perforated	245	320	76	3%
CB102	Plane	46	50	92	
E1660	Plane	110	118	94	

burning the trace. Reduced area caused by the gaps leads to higher resistance of trace generate the heat and destroy the trace itself by burning. Therefore, different current flux needs to pass through the ink trace to determine the ampacity.

In space, charging and discharging is a most common phenomenon which could damage the trace. Charging and discharging was simulated during the image acquisition in SEM by applying different electron beam intensities through ink traces to observe the change of ink surface structure. There was a similarity between simulated space environment and SEM chamber that had vacuum chamber to place the ECIs specimens. In both systems, air and gaseous molecules expelled from the chamber and create a vacuum. UV irradiation effect can be simulated using the electron beam gun in thermal vacuum system. Whereas in SEM different intensity electron beam passed through the sample to acquire the response to electron emission. Therefore, different electron beam intensity light was passed through the specimen to create the representative UV irradiation effect. There were no noteworthy changes between the ranges of 10kV to 35kV. Image, as shown in Figure 34, Figure 35, and *Figure 36* were taken at 30kV. Due to the bubble formation and afterward destruction on CB102 surface is inconvenient for space or vacuum medium application.

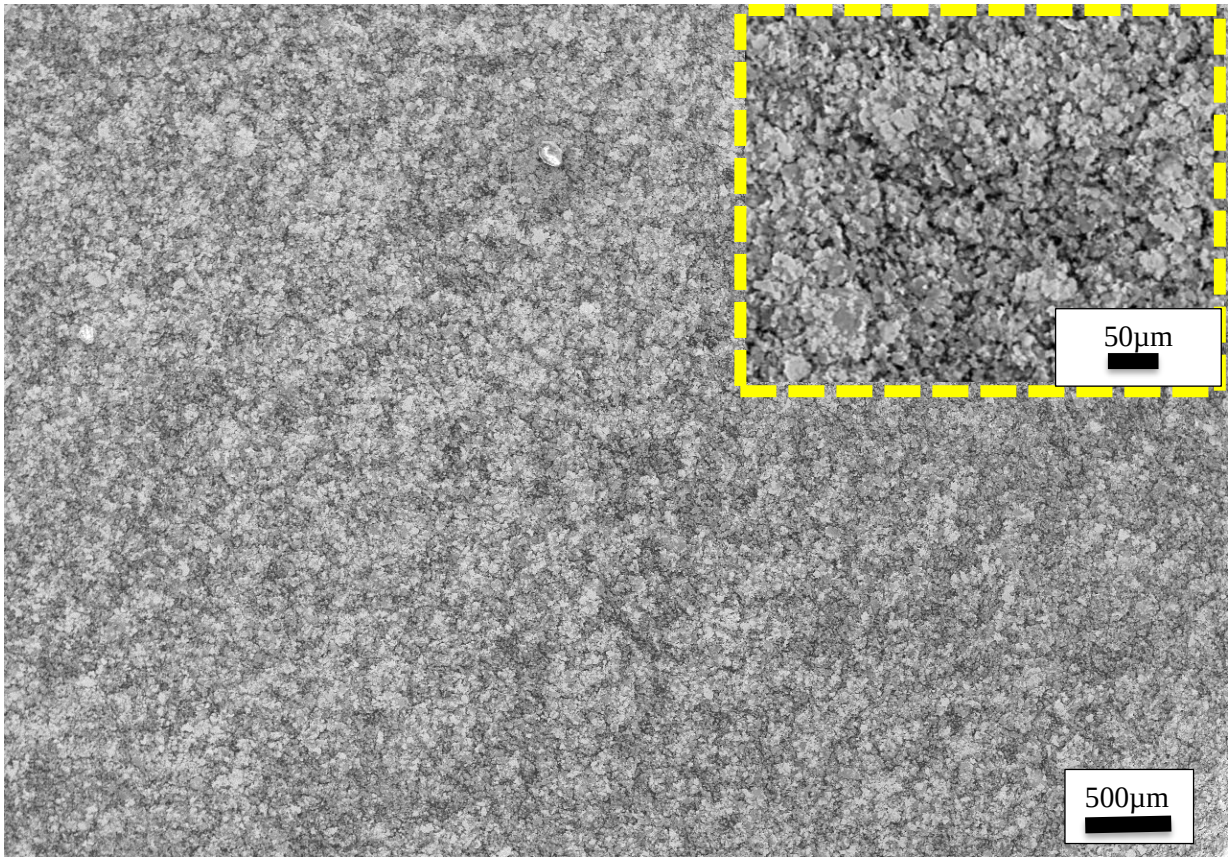

Figure 36: Microstructure of E1660 represents that there was no destruction of bubble. Silver flakes has heterogeneous size which can be seen in 50µm image. Accumulation of silver flakes conducted electricity and adhered to the PCB substrate as well.

While CB102 was experiencing the disturbance or irregularity on the surface structure, E1660 had given the more regular and well-structured surface. Interestingly, there was bubble formation followed by surface and bulk shrinkage, which leads to adhesion with the substrate material. Even though the SEM image in *Figure 36* represents the gap between flakes due to the evaporation of the solvent, still there was no such damage on the surface compared to the CB102. Since both samples were placed inside the chamber and removed from the chamber at the same time, CB102 had a deteriorated surface due to the bubble formation which proved that the E1660 is more promising for vacuum application.

Chapter 5: Conclusion and Recommendation

In this research possibility of the ECIs as extruder material of DW application in the simulated space environment were investigated. The key interest was the conductive behavior of two ECIs (Ercon E1660 and DuPont CB102) in the thermal vacuum system. The characterization parameter such as the development of a conductive path and time required to provide maximum current flow was first investigated at atmospheric pressure and room temperature. To validate the experimental setup and test procedure, elevated temperature and low temperature tests were performed using an Instron environment chamber. These tests were performed to demonstrate the continuity behavior of selected ECIs. The time required to develop a conductive path and resistance of ink traces after obtaining full continuity was measured by plotting the experimental data.

All tests were performed by dispensing the ECI using a commercial syringe. To demonstrate the automated dispensing system using conductive ink, a spring loaded micro dispenser was fabricated. Since the dispenser concept was for the space application, some parts of the dispenser (e.g. spring), were tested under a thermal system to determine the performance in the space environment. Testing of spring in thermal environment confirmed that the variation of the spring constant remained within the limit of the required spring constant. Other parts, such as O-rings and pin materials, were selected according to the space applicability requirements using the NASA low outgassing guide.

The thermal vacuum testing of ECI was performed using the vacuum chamber. This chamber test setup was modified for a low temperature (-70℃) and an elevated temperature (80℃). For each testing in the vacuum chamber, there was a time lapse from the ink dispensing time to

the start time of the vacuum pump. On average, the time required to close the chamber and run the vacuum system was 2 minutes for each test.

E1660 and CB102 had three most common difference in viscosity, polymeric binder (solvent), and conductive particles size. CB102 had a high viscosity (85Pa.s) that was responsible for premature curing or solidification of the binder at high temperature and room temperature. Premature and early solidification at room temperature and elevated temperature increased the risk of solidification before dispensing the ink from the dispenser. At elevated temperature (80℃) test in a vacuum chamber, CB102 created a conductive path within 200s, whereas the E1660 took approximately 225s to 300s. At room temperature (22℃), CB102 provided the continuity right after the dispensing on PCB substrate. At similar condition (22℃), E1660 provided the continuity after 750s (approximately 13 minutes). Early conductivity results of CB102 at room temperature indicated the premature solidification and curing. Premature solidification or hardening leads to clogging the ink inside the injector and orifice. In addition, premature curing and solidification reduce the shelf life.

Both of the inks created a conductive path at low temperature test in a vacuum chamber. At -20℃, E1660 took 1300s (approximately 22 minutes) to provide the continuity and CB102 took 2100s (approximately 35 minutes). For each test at low temperature (-20℃ to -70℃), E1660 created the conductive path in 60 to 65% of the time required by CB102. The low temperature environment was responsible for the delayed evaporation or solidification of solvent from the liquid ink.

Additionally, the physical appearance and morphology of ink traces were observed to investigate the topographical structure change after thermal vacuum testing. In all three-different thermal testing (room temperature, low and elevated temperature) CB102 had the damaged surface

due to the bubble formation and destruction. On the other hand, there was no such damage (no perforation as found in CB102) on E1660. The destruction of bubbles created perforations on the surface of the CB102 ink. Due to the evaporation of the polymer binder from the ink, gaps between silver particles were found. Gaps between conductive particles on the ink surface were measured using the LabVIEW machine vision tool. In the perforated section of the surface for CB102, the average area of the gap was 245μm^2. The rest of the plane surface (non-perforated) had the average gap area was 107μm^2. In other words, the gap between conductive particles in the perforated section was more than double of the gap in a plane surface. This bubble affected section also had 24% area of holes and gaps whereas the plane section had only 8% of holes and gaps. E1660 had plane surface i.e. there was no perforation. Since E1660 has flake based heterogeneous silver particles, there was an average gap area of 110μm^2 between conductive particles. Only 6% of the total surface area had the holes and 94% of the surface area had the conductive particles. Therefore, the high (94% as compared to the 76% of CB102) percentage of conductive particles on the surface of E1660 promoted the simultaneous evaporation and solidification of the binder from the ink surface and resulted in accumulated silver particles. As a result of silver particle accumulation, a conductive path was developed and conducted the electricity. It is important to bring attention to any space applicable materials that charging and discharging due to UV irradiation can damage and change material properties. During the SEM image acquisition, both ECI specimens were subjected to the simulated space environment because SEM chamber had a low pressure and charging-discharging environment. Charging and discharging were simulated using different intensity electron beams: 10kV, 15kV, 30kV, and 35kV. There was no change found on the morphology of both ECIs.

All the tests data generated from the atmospheric and thermal vacuum tests of CB102 and E1660 at three different temperatures (room temperature, low and elevated temperature) were indicated that the flake-based ECI has the potential for dispensing using DW technology in the space environment. At the end, material shelf life and curing properties in vacuum condition are the most important characteristics to consider as a space grade material. All the testing procedures and results successfully demonstrated the conductive behavior of ECI before and after developing a conductive path or curing. Though further testing is needed in a more sophisticated test facility that has a radiation environment, consistent temperature control and leak proof high vacuum chamber as the representative of simulated space environment, the information of this research work will help to select the materials to develop a repair kit using DW technology as well as future manufacturing in space environment.

Although this experimental study was performed in a thermal vacuum chamber that had the capability to create vacuum level of 10^{-2}Torr, more vacuum level can be created to simulate the deep space environment. This experimental procedure and test setup can be completely implemented in a high vacuum test facility. Further testing of ECI is needed to perform in such a test facility that has the ability of electron irradiation, electron gun, UV irradiation, thermal cycle, and vacuum level 10^{-5}Torr to 10^{-11}Torr. The charging and discharging effect could be explained in details by changing the trace thickness and dimensions in simulated space condition. Also, the test data of these experimental study can be used to compare with numerical modeling and analysis of ink curing mechanism at space environment. In future, it is possible to formulate a polymer binder to (a) evaporate or solidify at low temperature and create a conductive path by combining the conductive particles and (d) modify the shelf life for long term operational life.

References

[1]. Garcia. Mark, “Space Debris and Human Spacecraft.” [https://www.nasa.gov/mission_pages/station/news/orbital_debris.html]. July 2016.

[2]. Standard, NASA Safety. "Guidelines and assessment procedures for limiting orbital debris." NASA NSS 1740 (1995): 14.

[3]. Parazynski, S., and Wheelock, D., “Astronaut Scott Parazynski repairs a damaged ISS solar panel.” [https://www.nasa.gov/50th/favpic/parazynski.html]. August 2008.

[4]. Walters, R. J., T. L. Morton, and S. R. Messenger. "Displacement damage effects in solar cells—mining damage from the microelectronics and photonics test bed space experiment." NASA Tech. Rep., TP-2004 213338 (2004).

[5]. Gao, Xin, and Sheng-sheng Yang. "Radiation Effects of Space Solar Cells." High-Efficiency Solar Cells. Springer International Publishing, 2014. 597-622.

[6]. Fasooniehchi, A. R., and M. Taherbaneh. "A New Solar Cell Model for Evaluating Degradation of various il icon Cells at LEO and eO r its." Recent Advances in Space Technologies, 2007. RAST'07. 3rd International Conference on. IEEE, 2007.

[7]. Khan, Arifur R., Shiyi Chen, and Mengu Cho. "Charging and Discharging Phenomena of Plastic Encapsulated Microcircuits Used in Nanosatellites." Journal of Spacecraft and Rockets (2016): 1-9.

[8]. Brandhorst, Henry W., and Julie A. Rodiek. "Space solar array reliability: a study and recommendations." Acta Astronautica 63.11 (2008): 1233-1238.

[9]. Dearden, A. L., Smith, P. J., Shin, D.-Y., Reis, N., Derby, B. and O'Brien, P. (2005), A Low Curing Temperature Silver Ink for Use in Ink-Jet Printing and Subsequent Production

of Conductive Tracks. Macromol. Rapid Commun., 26: 315–318. doi:10.1002/marc.200400445

[10]. Eric A. Sanchez, Maike Waldmann, and Craig B. Arnold, "Chalcogenide glass microlenses by inkjet printing," Appl. Opt. 50, 1974-1978 (2011)

[11]. Mannoor, Manu S., et al. "3D printed bionic ears." Nano letters 13.6 (2013): 2634-2639.

[12]. Tribble, Alan, The Space Environment: Implications for Spacecraft Design, Princeton Univ Pres, 1995

[13]. Roth, Alexander. Vacuum technology. Elsevier, 2012.

[14]. Leigh, Simon J., et al. "A simple, low-cost conductive composite material for 3D printing of electronic sensors." PloS one 7.11 (2012): e49365.

[15]. Espalin, David, et al. "3D Printing multifunctionality: structures with electronics." The International Journal of Advanced Manufacturing Technology 72.5-8 (2014): 963-978.

[16]. Standard, A. S. T. M. "F2792-12a." Standard terminology for additive manufacturing technologies ASTM International, West Conshohocken, 2012.

[17]. Bourell, David L., David W. Rosen, and Ming C. Leu. "The roadmap for additive manufacturing and its impact." 3D Printing and Additive Manufacturing 1.1 (2014): 6-9.

[18]. Joe Lopes, Amit, Eric MacDonald, and Ryan B. Wicker. "Integrating stereolithography and direct print technologies for 3D structural electronics fabrication." Rapid Prototyping Journal 18.2 (2012): 129-143.

[19]. Medina, Frank, et al. "Hybrid manufacturing: integrating direct-write and stereolithography." Proceedings of the 2005 solid freeform fabrication (2005): 129-143.

[20]. Lee, Hsien-Hsueh, Kan-Sen Chou, and Kuo-Cheng Huang. "Inkjet printing of nanosized silver colloids." Nanotechnology 16.10 (2005): 2436.

[21]. Kamyshny, Alexander, Joachim Steinke, and Shlomo Magdassi. "Metal-based inkjet inks for printed electronics." The Open Applied Physics Journal 4.1 (2011).

[22]. Araki, Teppei, et al. "Printable and stretchable conductive wirings comprising silver flakes and elastomers." IEEE Electron Device Letters 32.10 (2011): 1424-1426.

[23]. Roberson, David Adrian. A novel method for the curing of metal particle loaded conductive inks and pastes. 2012.

[24]. Curtis, Calvin, et al. "Metallizations by direct-write inkjet printing." Proc. NCPV Program Rev. Meeting. 2001.

[25]. Roberson, David A., et al. "Microstructural and process characterization of conductive traces printed from Ag particulate inks." Materials 4.6 (2011): 963-979.

[26]. Mei, Junfeng, Michael R. Lovell, and Marlin H. Mickle. "Formulation and processing of novel conductive solution inks in continuous inkjet printing of 3-D electric circuits." IEEE transactions on electronics packaging manufacturing 28.3 (2005): 265-273.

[27]. Araki, Teppei, et al. "Printable and stretchable conductive wirings comprising silver flakes and elastomers." IEEE Electron Device Letters 32.10 (2011): 1424-1426.

[28]. Walker, S. Brett, and Jennifer A. Lewis. "Reactive silver inks for patterning high-conductivity features at mild temperatures." Journal of the American Chemical Society 134.3 (2012): 1419-1421.

[29]. Shin, Dong-Youn, Minhwan Jung, and Sangki Chun. "Resistivity transition mechanism of silver salts in the next generation conductive ink for a roll-to-roll printed film with a silver network." Journal of Materials Chemistry 22.23 (2012): 11755-11764.

[30]. Cesarano III, Joseph, and Paul D. Calvert. "Freeforming objects with low-binder slurry." U.S. Patent No. 6,027,326. 22 Feb. 2000.

[31]. Gratson, Gregory M., Mingjie Xu, and Jennifer A. Lewis. "Microperiodic structures: Direct writing of three-dimensional webs." Nature 428.6981 (2004): 386-386.

[32]. Lewis, Jennifer A., and Gregory M. Gratson. "Direct writing in three dimensions." Materials today 7.7 (2004): 32-39.

[33]. Hon, K. K. B., L. Li, and I. M. Hutchings. "Direct writing technology—Advances and developments." CIRP Annals-Manufacturing Technology 57.2 (2008): 601-620.

[34]. Ahmadloo, Majid, and Pedram Mousavi. "A novel integrated dielectric-and-conductive ink 3D printing technique for fabrication of microwave devices." Microwave Symposium Digest (IMS), 2013 IEEE MTT-S International. IEEE, 2013.

[35]. Li, Bo, Patrick A. Clark, and K. H. Church. "Robust direct-write dispensing tool and solutions for micro/meso-scale manufacturing and packaging." Proceedings of the ASME International Manufacturing Science and Engineering Conference. 2007.

[36]. https://www.micropen.com 2017

[37]. Lee, Hsien-Hsueh, Kan-Sen Chou, and Kuo-Cheng Huang. "Inkjet printing of nanosized silver colloids." Nanotechnology 16.10 (2005): 2436.

[38]. Kim, Dongjo, and Jooho Moon. "Highly conductive ink jet printed films of nanosilver particles for printable electronics." Electrochemical and Solid-State Letters 8.11 (2005): J30-J33.

[39]. Bai, John G., Kevin D. Creehan, and Howard A. Kuhn. "Inkjet printable nanosilver suspensions for enhanced sintering quality in rapid manufacturing." Nanotechnology 18.18 (2007): 185701.

[40]. Jung, Inyu, et al. "A simple process for synthesis of ag nanoparticles and sintering of conductive ink for use in printed electronics." Journal of electronic materials 41.1 (2012): 115-121.

[41]. Jeong, Sunho, et al. "Controlling the thickness of the surface oxide layer on Cu nanoparticles for the fabrication of conductive structures by ink-jet printing." Advanced Functional Materials 18.5 (2008): 679-686.

[42]. Lee, Youngil, et al. "Large-scale synthesis of copper nanoparticles by chemically controlled reduction for applications of inkjet-printed electronics." Nanotechnology 19.41 (2008): 415604.

[43]. Jeong, Sunho, et al. "Stable aqueous based Cu nanoparticle ink for printing well-defined highly conductive features on a plastic substrate." Langmuir 27.6 (2011): 3144-3149.

[44]. Park, Bong Kyun, et al. "Direct writing of copper conductive patterns by ink-jet printing." Thin Solid Films 515.19 (2007): 7706-7711.

[45]. Tam, Sze Kee, et al. "Product design: Metal nanoparticle-based conductive inkjet inks." AIChE Journal 62.8 (2016): 2740-2753.

[46]. Packirisamy, S., D. Schwam, and M. H. Litt. "Atomic oxygen resistant coatings for low earth orbit space structures." Journal of materials science 30.2 (1995): 308-320.

[47]. Banea, Mariana D., and Lucas FM da Silva. "Static and fatigue behaviour of room temperature vulcanising silicone adhesives for high temperature aerospace applications. Vol: 41.5 (2010): 325-335.

[48]. Morrissey, Susan R., “New Materials For Aging Space Shuttle.” [https://pubs.acs.org/cen/coverstory/83/8344NASA.html], October 2005.

[49]. Sbirrazzuoli, Nicolas, and Sergey Vyazovkin. "Learning about epoxy cure mechanisms from isoconversional analysis of DSC data." Thermochimica Acta 388.1 (2002): 289-298.

[50]. Honig, Richard E., and Dean A. Kramer. "Vapor-pressure data for the solid and liquid elements." (1970).

[51]. Jeong, Woo-Ju, et al. "Effect of solvent evaporation and shrink on conductivity of conductive adhesive." Materials transactions 46.3 (2005): 704-708.

[52]. http://chemed.chem.purdue.edu/genchem/topicreview/bp/ch14/clausius.php

[53]. Rhodes, Martin J. Introduction to particle technology. John Wiley & Sons, 2008.

[54]. Note, Dimatix Application. "Dimatix materials printer: jettable fluid formulation guidelines."

[55]. James, Bonnie F., O. W. Norton, and Margaret B. Alexander., The Natural Space Environment: Effects on Spacecraft, NASA STI/Recon Technical Report N 95 (1994): 25875.

[56]. ASTM E1559, Standard Test Method for Contamination Outgassing Characteristics of Spacecraft Materials.

[57]. ASTM E595, Standard Test Method for Total Mass Loss and Collected Volatile Condensable Materials from Outgassing in a Vacuum Environment.

[58]. Cengel, Yunus A., and Michael A. Boles. "Thermodynamics: an engineering approach." Sea 1000 (2002): 8862.

[59]. https://www.nasa.gov/sites/default/files/files/NP-2015-03-015-JSC_Space_Environment-ISS-Mini-Book-2015-508.pdf

[60]. Barth, Janet L., C. S. Dyer, and E. G. Stassinopoulos. "Space, atmospheric, and terrestrial radiation environments." IEEE Transactions on Nuclear Science 50.3 (2003): 466-482.

[61]. Zell, Holly, “Radiation Belts with Satellites.” [https://www.nasa.gov/mission_pages/sunearth/news/gallery/20130228-radiationbelts.html]. February 2013.

[62]. Duzellier, Sophie. "Radiation effects on electronic devices in space." Aerospace science and technology 9.1 (2005): 93-99

[63]. Fleetwood, Daniel M., Peter S. Winokur, and Paul E. Dodd. "An overview of radiation effects on electronics in the space telecommunications environment." Microelectronics Reliability 40.1 (2000): 17-26.

[64]. Howard Jr, J. W. Spacecraft environments interactions: Space radiation and its effects on electronic systems. National Aeronautics and Space Administration, Marshall Space Flight Center, 1999.

[65]. http://www.cdn.sciencebuddies.org/Files/4810/6/fig9_multimeter-continuity-test-beep.jpg

[66]. Sourour, S., and M. R. Kamal. "Differential scanning calorimetry of epoxy cure: isothermal cure kinetics." Thermochimica Acta 14.1 (1976): 41-59.

[67]. Roberson, David A., R. B. Wicker, and E. MacDonald. "Ohmic curing of printed silver conductive traces." Journal of electronic materials (2012): 1-14.

[68]. Lopes, Amit J., et al. "Laser curing of silver-based conductive inks for in situ 3D structural electronics fabrication in stereolithography." Journal of Materials Processing Technology 214.9 (2014): 1935-1945.

[69]. Ercon E1660 Technical Data Sheet (Wareham, MA: Ercon Inc., 2007), p. 1.

[70]. DuPont CB028 Silver Conductor Technical Data Sheet (Wilmington, DE: DuPont, 2009).

[71]. Thurn, Adam, et al. "A Nichrome burn wire release mechanism for CubeSats." The 41st Aerospace Mechanisms Symposium. 2012.

[72]. NASA, “Low gassing materials list”. [https://outgassing.nasa.gov/]. July 2017.

[73]. Werner, Brian T., Bonnie R. Antoun, and George B. Sartor. "Thermal Degradation of Extension Springs." Challenges in Mechanics of Time Dependent Materials, Volume 2. Springer International Publishing, 2016. 1-9.

[74]. King, David A. "Thermal desorption from metal surfaces: A review." Surface Science 47.1 (1975): 384-402.

Vita

Kazi Md Masum Billah was born on September 18, 1991. He is the son of Kazi Md Mofazzal Hossain and Mosa Nurun Nahar. Kazi completed his Bachelor of Science in Mechanical Engineering in September 2013 from the Khulna University of Engineering & Technology, Khulna, Bangladesh. He received a technical scholarship from the Khulna University of Engineering & Technology. He worked as a lecturer in World University of Bangladesh and a Teaching Assistant at The University of Texas at El Paso (UTEP). Kazi helped undergraduate students in research, hosted training sessions of different lab equipment and software. He also engaged himself actively on UTEP CubeSat research team that won the ULA CubeCorp competition. Kazi and his team member were recognized by Texas house of representative at the capitol of Texas, Austin 2017.

Permanent address: Village: Shotahar Kazi Para Post Office: Darki
Police Station: Joypurhat Sadar, District: Joypurhat, Country: Bangladesh

This thesis was typed by Kazi Md Masum Billah.